A PERMANENT-MAGNET MICROWAVE DISCHARGE ION SOURCE AT KAHVELAB

by

Sevim Açıksöz

B.S., Physics, Boğaziçi University, 2019

Submitted to the Institute for Graduate Studies in
Science and Engineering in partial fulfillment of
the requirements for the degree of
Master of Science

Graduate Program in Physics

Boğaziçi University

2022

ACKNOWLEDGEMENTS

This studies were supported by TÜBİTAK under the project grant 119M774 “Düşük Enerjili Proton Demeti Için Ölçüm Kutusu Tasarımı ve Üretimi, Testleri” which is funded by TUBITAK 3501. Also, during these studies I have been financially supported by “TÜBİTAK 2210-A Genel Yurt İçi Yüksek Lisans Burs Programı 2020/2”.

I would like to express my deepest gratitude to Hakan Çetinkaya and Sinan Öz for their dedicated contributions to this study. Hakan has provided guidance and feedback patiently throughout this study, he always believed me and made me feel confident in my abilities. Then, I would like to thank Gökhan Ünel, Veysi Erkcan Özcan for their motivating inspiration and support, and Aytul Adiguzel for her extraordinary efforts as a project executive. I would also like to thank Gökhan and Salim for carrying the magnets from thousands of kilometers away. It would have been definitely impossible to complete this work without their help. I am grateful to everyone that we have collaborated with in KAHVELab.

ABSTRACT

A PERMANENT-MAGNET MICROWAVE DISCHARGE ION SOURCE AT KAHVELAB

A new Permanent Magnet Microwave Discharge Ion Source (PM-MDIS) has been designed and constructed at Boğaziçi University Kandilli Detector, Accelerator, and Instrumentation Laboratory (KAHVELab). The PM-MDIS design includes a plasma chamber surrounded by permanent magnets, a hydrogen gas supply to sustain the plasma, the waveguide system used to transfer power to the plasma chamber, a dual-electrode extraction system used to extract ions from the chamber, and a Faraday cup to measure the beam current. The aim is to extract ions from the thermal hydrogen plasma generated using a 2.45 GHz microwave source. In order to extract ions from the plasma medium, a magnetic field exceeding 875G has to be applied over the plasma chamber to ensure Electron Cyclotron Resonance (ECR) condition is satisfied. Since the plasma chamber is to be operated on the high voltage (HV) platform, higher system stability can be achieved by using the permanent magnet configuration shown in this work. Based on the designed magnetic field profile of the constructed system, the dual-electrode extraction system has also been designed using IBSIMU integrated DemirciPro software and produced to transmit proton beams from the plasma chamber to the beamline. The determination of the magnetic field profile, and the vacuum, HV, and beam tests are completed before integration with the rest of the beamline. Finally, how the transmitted proton beams behaved on the existing Low Energy Beam Transport (LEBT) line has been examined, and the LEBT line configuration has been optimized accordingly. In addition, besides the protons, the trajectories of H_2^+ and H_3^+ ions from the PM-MDIS have also been studied to optimize the LEBT beam optics. As a result of this study, the PM-MDIS has been integrated with the proton beamline, and 0.38 mA mean beam current has been measured with the Faraday cup in the experiments performed at 20 kV and 0.01 sccm gas flow.

ÖZET

KAHVELAB KALICI MIKNATISLI MİKRODALGA DEŞARJ İYON KAYNAĞI

Boğaziçi Üniversitesi Kandilli Dedektör, Hızlandırıcı ve Enstrümantasyon Laboratuvarı'nda (KAHVELab) yeni bir Kalıcı Mıknatıslı Mikrodalga Deşarj İyon Kaynağı (PM-MDIS) tasarlanmış ve üretilmiştir. PM-MDIS tasarımı, sabit mıknatıslarla çevrili bir plazma odası, plazmayı sürdürmek için bir hidrojen gazı kaynağı, gücü plazma odasına aktarmak için kullanılan dalga kılavuzu sistemi, odadan iyonları çıkarmak için kullanılan çift elektrotlu bir sökme sistemi ve demet akımını ölçmek için bir Faraday kabı içerir. Amaç, 2.45 GHz mikrodalga kaynağı kullanılarak üretilen termal hidrojen plazmasından iyonları çekmektir. Plazma ortamından iyonları çıkarmak için, plazma odası boyunca Elektron Siklotron Rezonans (ECR) koşulunu sağlayacak, 875G'yi aşan bir manyetik alan uygulanmalıdır. Plazma odası yüksek voltaj altında çalıştırılacağından, bu çalışmada gösterilen kalıcı mıknatıs konfigürasyonu kullanılarak daha yüksek sistem kararlılığı sağlanabilir. Kurulan sistemin tasarlanan manyetik alan profiline dayalı olarak, çift elektrotlu iyon sökme sistemi de IBSIMU entegre edilmiş DemirciPro yazılımı kullanılarak tasarlanmış ve proton demetini plazma odasından demet hattına iletmek üzere üretilmiştir. Manyetik alan profilinin belirlenmesi, vakum, yüksek voltaj ve demet testleri, demet hattının geri kalanıyla entegrasyonundan önce tamamlanmıştır. Son olarak, iletilen proton demetinin mevcut Düşük Enerjili Demet Taşıma (LEBT) hattı üzerinde nasıl davrandığı incelenmiş ve LEBT hattı konfigürasyonu buna göre optimize edilmiştir. Ek olarak, protonların yanı sıra, LEBT demet optiklerini optimize etmek için PM-MDIS'ten H_2^+ ve H_3^+ iyonlarının hareketleri de incelenmiştir. Bu çalışma sonucunda, PM-MDIS proton demet hattı ile entegre edilmiş ve 20 kV ve 0.01 sccm gaz akışında gerçekleştirilen deneylerde 0.38 mA ortalama demet akımı Faraday kabı ile ölçülmüştür.

TABLE OF CONTENTS

LIST OF FIGURES

LIST OF TABLES

LIST OF SYMBOLS

A	Ampere
B	Magnetic Field
c	Speed Of Light
C	Celsius
d	Distance
E	Electric Field
eV	Electron Volt
f	Frequency
F	Force
h	Planck Constant
H	Hydrogen
H^-	Hydrogen Anion (Hydride)
H^+	Hydrogen Cation (Hydron)
H_2^+	Dihydrogen Cation
H_3^+	Trihydrogen Cation
Hz	Hertz
I	Current
J	Current Density
kV	Kilovolts
mA	Milliampere
mbar	Millibar
mm	Millimeter
mrad	Milliradian
N	North Pole
P	Pressure
q	Charge
q_e	Charge Of The Electron
r	Radius
R	Resistance

RMS	Root Mean Square
sccm	Standard Cubic Centimeter Per Minute
S	South Pole
t	Time
T	Tesla
U	Applied Potential
V	Volt
W	Watt
π	Pi
μA	Micro Ampere
λ	Wavelength
Φ	Ionization Potential
ω	Angular Velocity
υ	Velocity
$^\circ$	Degree
Δ	Change In Quantity
Ω	Ohm

LIST OF ACRONYMS/ABBREVIATIONS

AC	Alternating Current
CNC	Computer Numerical Control
CRNL	Chalk River National Laboratory
DC	Direct Current
ECR	Electron Cyclotron Resonance
ECRIS	Electron Cyclotron Resonance Ion Source
FEM	Finite Element Method
FDM	Finite Difference Method
HV	High Voltage
KAHVELab	Kandilli Detector, Accelerator, and Instrumentation Laboratory
LEBT	Low Energy Beam Transport
MBOX	Measurement Box
MDIS	Microwave Discharge Ion Source
PM	Permanent Magnet
PM-MDIS	Permanent Magnet Microwave Discharge Ion Source
PSU	Power Supply Unit
RF	Radio Frequency
RFQ	Radio Frequency Quadrupole
TE	Transverse Electric Field Mode
TM	Transverse Magnetic Field Mode

1. INTRODUCTION

At the Boğaziçi University Kandilli Detector, Accelerator, and Instrumentation Laboratory (KAHVELab), there is an ongoing project to build and operate an 800 MHz RFQ, that would accelerate beams with a current of approximately 1 mA up to 2 MeV [1]. The proton beamline of this accelerator starts with a Microwave Discharge Ion Source (MDIS) operating at the 2.45 GHz frequency to create hydrogen plasma and to obtain a proton beam at 20 keV energy with the electrode extraction system. Proton beams are formed by satisfying the ECR condition [2, 3] with a certain magnetic field profile. The proton beam extracted from the MDIS is transferred to the RFQ cavity and needs to satisfy the $0.2\,\pi$.mm.mrad emittance value requirement at the entrance to the RFQ [4]. Proton beam is transferred through the Low Energy Beam Transport (LEBT) line, comprising two solenoid magnets, two steerer magnets, and a beam diagnostic box (MBOX) between these electromagnets. The beam diagnostic box, including a Faraday cup, a pepper pot plate, and a home-built scintillator screen, is designed to measure the current, emittance, and profile of the incoming beam to ensure the required beam matching between MDIS output and RFQ input. The overall scheme for the KAHVELab proton beamline can be seen in Figure 1.1, and the current operating setup for MDIS, LEBT, and MBOX can be seen in Figure 1.2.

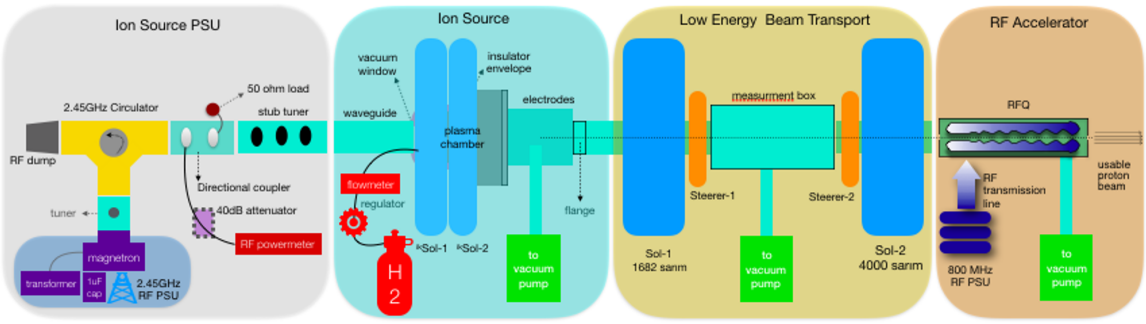

Figure 1.1. The scheme for proton testbeam line at KAHVELab.

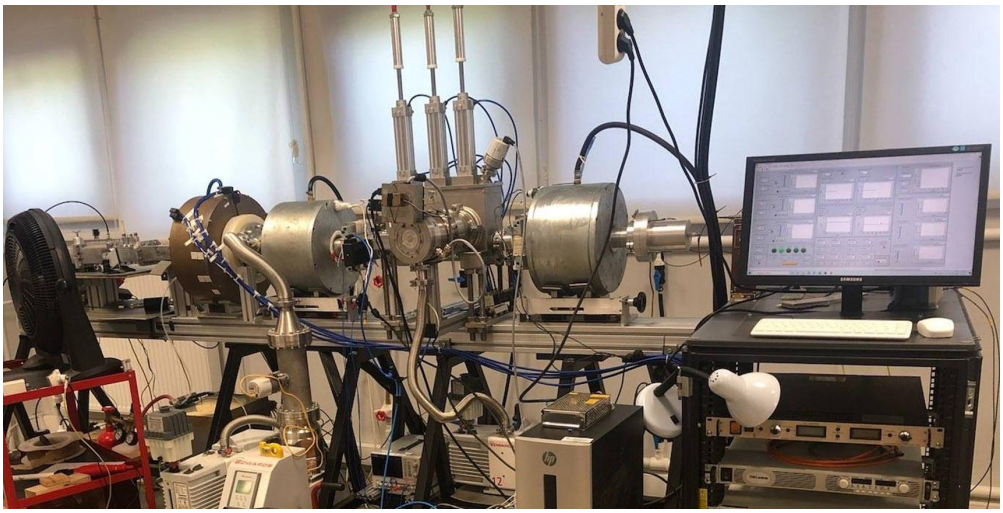

Figure 1.2. Overall setup for the ion source unit, LEBT line and the beam diagnostics box.

The MDIS is the first part of this linear accelerator. For its successful operation at 2.45 GHz source frequency, a minimum 875 Gauss magnetic field is required to satisfy the ECR state and achieve optimal condition for plasma density [2, 3, 5]. The existing ion source setup operates with electromagnets to achieve this required magnetic field profile. The electromagnet system consists of 2 solenoids, 525 turns each, and is placed around the plasma chamber. A general setup scheme for this ion source is given in Figure 1.3. This scheme includes a 2.45 GHz magnetron circuit as a microwave source, a microwave transmission system (including magnetron head, stub tuner, WR340 to WR284 waveguide transition, DC break which prevents HV transfer from plasma chamber to waveguide system), a fused quartz silica vacuum window which allows wave propagation of microwave from air to vacuum and it is also used as vacuum break, the plasma chamber, an electrode extraction system for protons, the alumina insulator between the plasma chamber and the electrode part, the solenoid system which covers the plasma chamber, and the Faraday cup. In an electromagnetic ion source system, solenoids need to be cooled because carrying current and the plasma chamber cause it to heat up. In this existing ion source setup, electromagnets require an extra current supply and a water cooling system, which means extra cost and higher maintenance for the project. Moreover, as they are placed around the plasma chamber,

they may occasionally cause sparks. Either the entire system will have to be kept under high voltage (HV), or an insulation layer between the plasma chamber and electromagnets will be required to prevent sparks. In the current electromagnet system, insulation material is used between solenoids and the plasma chamber to prevent sparks, but it is not shown in Figure 1.3. Unfortunately, the insulation tends to lose its property over time due to the heat, increasing the frequency of occurrence of sparks.

It has been decided to construct a new ion source with permanent magnets as an alternative to the current electromagnetic system as the permanent magnets can safely be kept under HV and do not require any additional current supply or HV insulation between magnets and the plasma chamber. We argue that it is possible to achieve a more stable and cost-efficient setup using this approach.

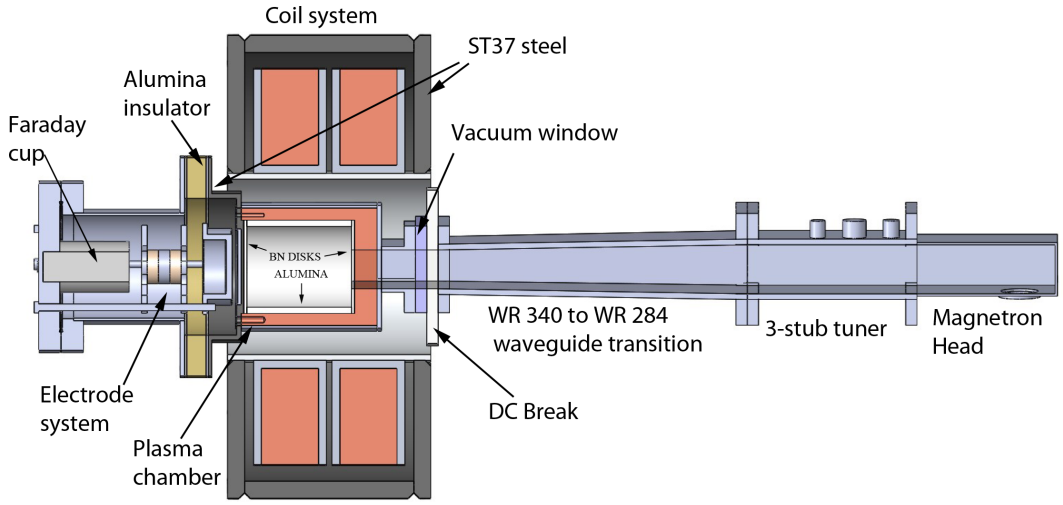

Figure 1.3. A scheme for the MDIS with electromagnets [6].

To transmit proton beams from the plasma chamber to the beamline, a 20 kV dual-electrode extraction unit has been designed. It has been optimized to ensure beam matching between MDIS and RFQ. The design of the MDIS electrodes is based on the magnetic field profile of the new ion source system with permanent magnets. Further analysis has been conducted for the trajectories of the dihydrogen and trihydrogen cation ions contained in the incoming beam to examine their possible effects on the

LEBT efficiency. The current system's LEBT configuration has been upgraded for the magnetic field profile of the new setup and its beam properties.

In this thesis, ion sources will be described in Chapter 2, magnetic field design studies for a new permanent magnet microwave discharge ion source (PM-MDIS) will be discussed in Chapter 3, and its electrode extraction unit design will be covered in Chapter 4. Then, its HV, vacuum, and beam tests will be the topics of Chapter 5.

2. ION SOURCES

Electric and magnetic fields are used to manipulate the trajectory of a particle through a direction with a velocity. Yet, the particle must be brought into a charged state to be affected by an electric and magnetic field. Ion sources are devices used to ionize particles and form atomic or molecular ion beams. Ion beams are generally extracted from plasma, and ion sources are used to extract and form ion beams from generated plasma medium for various purposes such as scientific experiments, industry, and medical applications. These devices are the primary unit for the systems working with charged particle beams. Mass spectrometers, surface treatments, and particle accelerators are some principal applications of ion sources. Certain specifications and optimizations required by varied application types have resulted in diverse ion source types. Ion source types are mainly classified according to their ion formation procedure. Several of them can be listed as:

- electron impact ion sources,
- photo-induced ion sources,
- negative ion sources,
- surface ion sources,
- radio frequency (RF) discharge ion sources,
- microwave ion sources.

Although there are diverse types of ion sources, an ion source essentially consists of the following parts:

- *Power Supply:* Ionization processes require a certain level of energy. The power source is necessary to provide this energy to the system.
- *Ionization chamber:* It is a vacuum chamber where the plasma forms; therefore, the ionization process takes place. It should be kept under vacuum to prevent plasma and ionized material contamination.
- *Extraction unit:* This part attracts ions from the chamber by applying an electric

field. Thus, the extracted beam is accelerated to a certain initial energy.

A generalized scheme for an ion source is represented in Figure 2.1. Operating an ion source requires additional components such as power supplies and vacuum pumps.

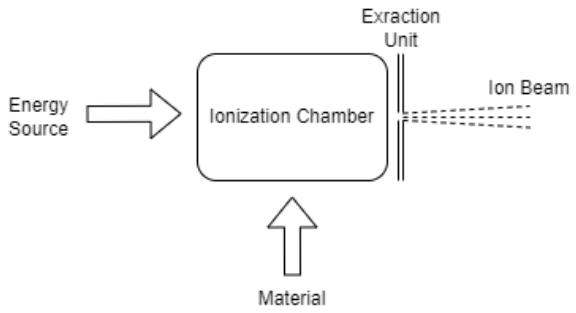

Figure 2.1. The simplified scheme for an ion source.

Some ion source types are described in the following setions. In this study, the aim is to extract H^+ ion beams to be accelerated through the RFQ cavity. It is desirable to choose an ion source type that is as stable as possible, has long lifetime, is low-cost, and simple, but can also provide proton beams to satisfy RFQ input matching requirements. To match KAHVELab's RFQ input, an emittance of $0.2\,\pi$.mm.mrad and a minimum beam current of about $1\,\mu$A is needed.

2.1. Surface Ion Sources

The surface ion source typically includes a filament which is heated to high degrees, and gas to be ionized. The gas is directed toward the heated filament, where ionization will occur. This procedure works effectively when the gas has low ionization energies and the filament has a high work function [7]. In some applications, the filament is designed as a tube that will be injected with gas to be ionized. A sample drawing for a surface ion source with a heated tube is given in Figure 2.3.

The lifespan of a surface ion source depends on its filament. While the lifespan of the filament depends on the beam current it draws. As the filament life expires,

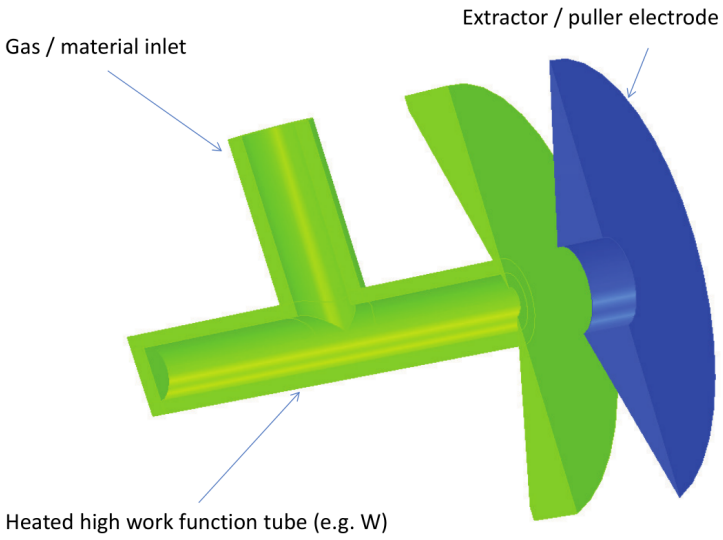

Figure 2.2. A sample drawing for a surface ion source with heated tube [7].

it requires some maintenance and eventually a replacement. This ion source type can provide high current negative and positive ion beams.

2.2. Laser Ion Sources

Laser ion sources use intense high-brightness laser beams. They are of two separate types: laser ionization ion sources and laser plasma ion sources. In the laser ionization type, ionization is generated directly by photons with the energy meeting the ionization potential energy. The required wavelength (λ) is calculated as

$$\lambda = \frac{hc}{q_e \Phi} \tag{2.1}$$

where h represents the Planck Constant, c is the speed of light, q_e is the charge of the electron, and Φ is the ionization potential.

From Equation (2.1), the suitable wavelength, even for the element with the lowest potential, is far beyond the ultraviolet lights. For this reason, multiple photons are used to ionize an atom. Photon impact ionization allows selectivity in the ionization process as the different atoms require different levels of excitation and ionization potential energy [7].

Laser plasma ion sources generate plasma by using intense radiation focused by mirrors or lenses from a laser source. When the laser hits on the solid target, it is easily vaporized and plasma is created. To generate plasma, resonance condition should be ensured between laser frequency and plasma electron oscillation frequency. Laser ion sources generally use a solid target to produce ion beams, which allows a wide range of ion types to be produced [7]. The main difference between two laser ion source type is that the laser ionization source ionization directly occurs by using the laser at the appropriate frequency, while the laser plasma source uses the high-power laser to create plasma and provide the resonance condition. This type of ion source is used to produce high charge state beams, but beam currents are generally low [2] [8].

2.3. Radio Frequency (RF) Discharge Ion Sources

RF discharge ion sources use a time-varying electric field to provide the required energy for ionization instead of a constant electric field applied by DC discharge ion sources. They can be used to ionize any type of gas. Some types of gases, such as oxygen, are not suitable to use with filaments due to oxidation. However, those kinds of gases can be safely ionized with RF discharge ion sources. Operating RF frequency can change from a few megahertz to tens of megahertz [9]. In this type, ionization can occur in two ways: capacitively coupled discharge and inductively coupled discharge. In the capacitively coupled discharge types, an alternating potential is applied between two parallel plates to generate a time-varying alternating electric field over the ionization chamber. A general scheme for a capacitively coupled system is shown in Figure 2.3.

In an inductively coupled system, discharge is generated by an alternating magnetic field provided by an induction coil or RF antenna. An alternating magnetic field is used to induce the electric field for ionization. A general scheme for an inductively coupled RF ion source system is given in Figure 2.4. RF antenna can be placed inside or outside the ionization chamber. According to antenna placement, the sources are classified as external RF antenna or internal RF antenna systems. RF ion sources can be used to produce positive and negative ion beams. A sample external RF antenna driven H^- ion source from the Spallation Neutron Source [7,10] is shown in Figure 2.5.

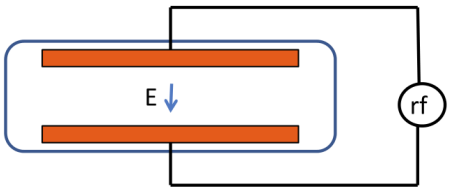

Figure 2.3. A simplified scheme for a capacitively coupled RF discharge ion source [7].

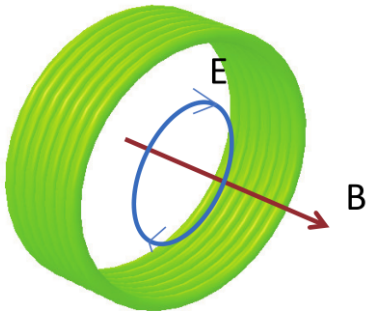

Figure 2.4. A simplified scheme for an inductively coupled RF discharge ion source [7].

2.4. Microwave Ion Sources

Unlike most other ion source types, microwave ion sources do not contain an apparatus to heat the gas to generate plasma inside the plasma chamber, such as a filament or internal radio frequency (RF) antenna. Thus, microwave ion sources have an extended lifespan and require less maintenance in operation as they do not require filament part replacements that can interrupt operation for a long time.

Microwave ion sources are mainly classified into Electron Cyclotron Resonance Ion Source (ECRIS) and Microwave Discharge Ion Source (MDIS). Operation principles of both of these ion source types are based on the electron cyclotron resonance condition.

2.4.1. Electron Cyclotron Resonance (ECR)

When a magnetic field, $\vec{B}$, is applied to a free electron of charge q_e, moving with velocity $\vec{v}$, the electron will rotate in a circular trajectory due to the Lorentz force with

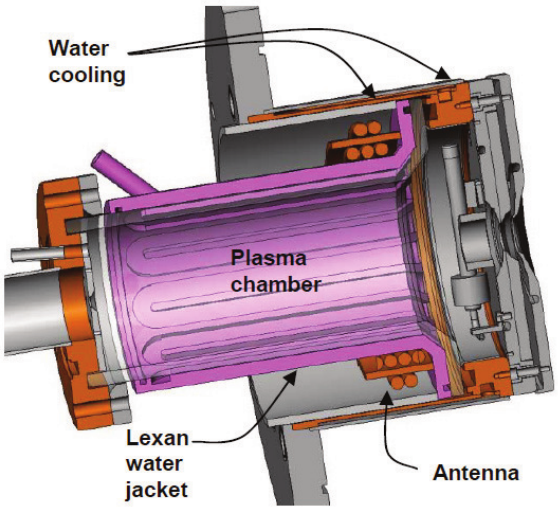

Figure 2.5. An example external RF antenna driven H^- ion source from the Spallation Neutron Source [7].

a uniform cyclotron frequency. The Lorentz Force is written as

$$\vec{F}_{Lorentz} = q_e(\vec{v} \times \vec{B}). \tag{2.2}$$

The magnetic field does not affect the particle motion in the direction of itself, and then it can be simplified as

$$F_{Lorentz} = q_e \upsilon B \tag{2.3}$$

$$F_{Lorentz} = q_e \omega r B \tag{2.4}$$

where ω is the angular velocity, and r is the radius of the particle's motion. The required magnetic field value to satisfy the resonance condition for a cyclotron frequency, f, can be obtained by equating the Lorentz force with the centripetal force, as

$$F_{Centripetal} = \frac{m\upsilon^2}{r} = m\omega^2 r \tag{2.5}$$

$$q_e \omega r B = m\omega^2 r \tag{2.6}$$

$$B = \frac{m\omega}{q_e} \tag{2.7}$$

$$B = \frac{m2\pi f}{q_e} \tag{2.8}$$

where m is the mass of the particle.

For a 2.45 GHz microwave source, the required B_{ECR} value to obtain cyclotron resonance can thus be calculated as

$$B_{ECR} \approx 0.0875\,T. \tag{2.9}$$

2.4.2. Electron Cyclotron Resonance Ion Sources (ECRIS)

The working principle of the ECRIS requires certain magnetic field zones ensuring electron cyclotron resonance with the electromagnetic energy inside the plasma chamber. These sources consist of two or three ring magnets to create an axial magnetic field and hexapole magnets to create a radial magnetic field [2], so there will be various field regions over the plasma chamber. The magnetic field profile allows satisfying ECR condition for the electrons heated by a microwave source to create plasma.

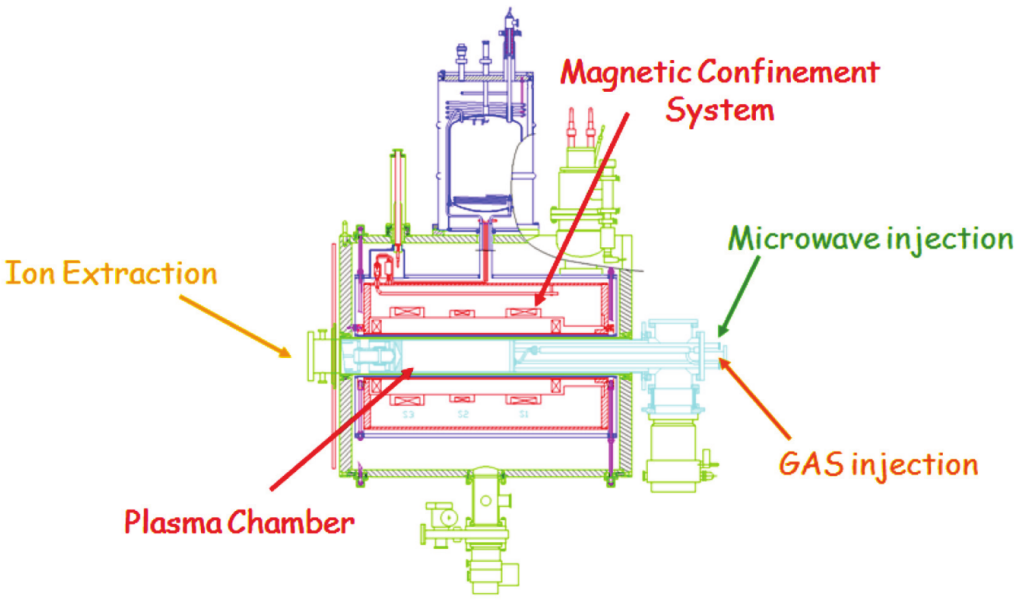

Figure 2.6. Main parts of an ECRIS [11].

Magnetic field zones in an ECRIS provide effective plasma confinement and higher temperatures allowing more energetic collisions, which result in multiple collisions and

multiply charged ions at the extraction. ECRIS can create high currents and higher charge states even in relatively low plasma pressure. However, creating magnetic confinement zones requires high plasma density [2, 8]. Designing a magnet configuration to be used by an ECRIS is a challenging process as it needs multiple distinct magnetic field profiles and very high magnetic field values throughout the entire chamber, accordingly an expensive and complex magnetic structure. A general scheme for an ECRIS is shown in Figure 2.6. Another example for ECRIS structure and field profile, designed by R.Geller in 1991 [12], is shown in Figure 2.7.

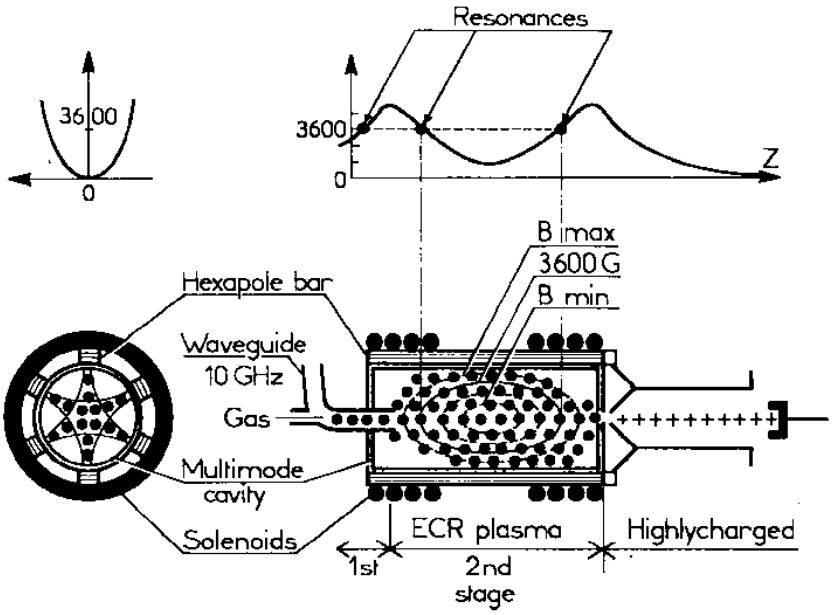

Figure 2.7. Scheme for the ECRIS designed by R. Geller in 1991 [12].

ECRISs have many advantages in creating highly charged particles. However, using ECRISs to extract singly charged ion beams is not deemed very suitable for our project, given its complex field requirements.

2.4.3. Microwave Discharge Ion Sources (MDIS)

A microwave discharge ion source (MDIS) is also an electron cyclotron resonance (ECR) condition-based ion source type. The main difference between MDIS and ECRIS types is the magnetic field profile which affects the plasma creation mechanism for a microwave ion source. While the ionization procedure of an ECRIS is based on magnetic confinement by creating confinement and resonance zones through the plasma chamber, MDIS has a non-confinement based magnetic field profile to create ion beams. Non-confinement in the magnetic field implies that the magnetic field (B) is either smaller or greater than B_{ECR} across the plasma chamber. Today, there are no high current ion sources that meet the $B < B_{ECR}$ requirement [13]. MDIS operates on the $B > B_{ECR}$, non-confinement basis field requirements. MDIS has a more simple magnetic structure than ECRIS, and it only needs an axial magnetic field to create singly charged ions, and no complex confinement zones. ECRISs are generally used to create highly charged particles by multiple ionization stages, and MDISs are preferred to create singly charged particles.

A 2.45 GHz MDIS was firstly proposed by Sakudo at the Central Research Laboratory of Hitachi in 1978 [14]. This study provided a high-current ion source for industrial applications. In 1991, an MDIS design, which forms a simple basis for today's machines, was proposed by Taylor and Mouris at Chalk River National Laboratory (CRNL) [15]. Figure 2.8 gives the scheme for the MDIS designed by Taylor and Mouris at CRNL, and its magnetic field profile on the central axis of the solenoids as a function of the distance [15] is given in Figure 2.9.

MDISs can provide high current and high brightness beams even in low plasma pressure with high reliability and do not require much effort for operation and maintenance. At KAHVELab, it is aimed to extract H^+ ions from hydrogen gas to form a proton beam that would be accelerated through the RFQ beamline. We have preferred to choose an ion source type that is as stable as possible, long-lifetime, low-cost, and not complex in design. An MDIS-type ion source to produce proton beams when considered in the following extends. It does not contain a filament or internal RF

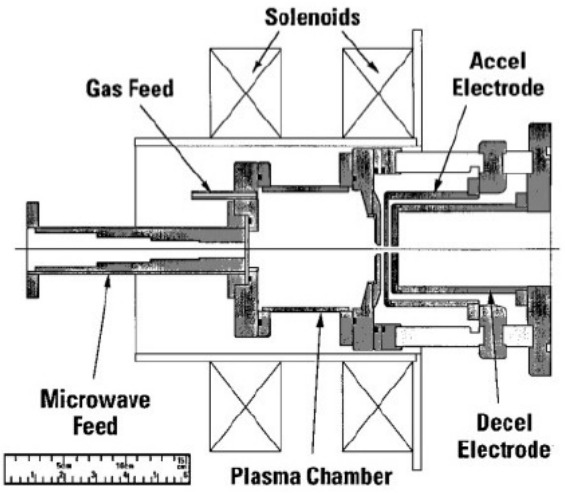

Figure 2.8. Scheme for the MDIS designed at CRNL at 1991 [15].

antenna inside the ionization chamber to generate plasma. This prevents operation interruptions due to filament part replacements, provides a long lifespan, and requires less maintenance for the project. It does not require a complex field structure to design; therefore, it is cost-efficient and ensures high reliability.

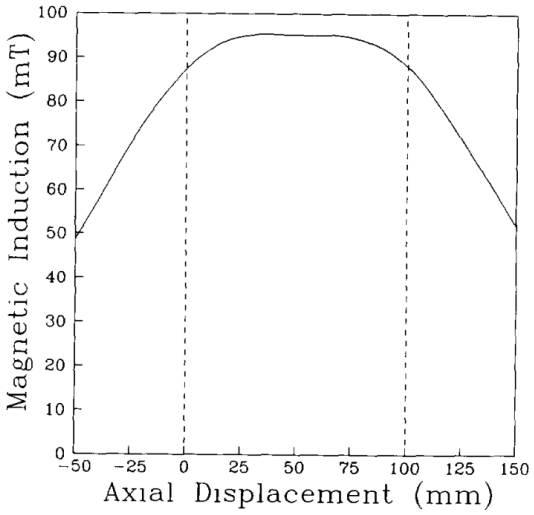

Figure 2.9. CRNL magnetic field profile on the central axis of the solenoids as a function of the distance from the microwave window, dashed lines represents plasma chamber location [15].

3. MAGNETIC FIELD DESIGN

The MDIS type meets our requirements for stablity and long operation life. The plasma is made electrically and confined magnetically [8]. An axial magnetic field is required throughout the ionization chamber to create thermal hydrogen plasma using a microwave source.

3.1. Field Constraints

The magnetic field requirement for the electron cyclotron resonance (ECR) condition is 875 Gauss for a 2.45 GHz microwave source as calculated in Equation (2.9). A microwave discharge ion source operates stably if the magnetic field provided through the plasma chamber exceeds the ECR value. To obtain higher plasma density, the optimal range is in between B_{ECR} and $1.3 \times B_{ECR}$ [16], which corresponds to 875 Gauss $<$ B $<$ 1137 Gauss for 2.45 GHz microwave source frequency. Besides, 820 Gauss has to be supplied at the waveguide-plasma chamber junction to ensure the active wave mode [3, 13, 17]. Therefore, the magnetic field value must be 820 Gauss at the plasma chamber entrance and above 875 Gauss across the plasma chamber, corresponding to the ECR requirement. If the magnetic field is strong on the beamline side, it will affect the path of the ions. A different beam path/electrode system design is required for each profile. Therefore, to eliminate the influence of the magnetic profile on the beamline, the magnetic field at the end of the plasma chamber (beginning of the electrodes) should be reduced to a value close to ~ 0 Gauss [13].

To create proton beams satisfying conditions for RFQ input matching and the required magnetic field profile based on the field constraints, two different magnet and electrode extraction systems have been designed & produced: an existing electromagnetic system and a system with permanent magnets.

3.2. The Existing MDIS Design With Electromagnets And Its Field Properties

There is an existing MDIS system [13] that has been operated to produce proton beams for the beamline for the last couple of years. This MDIS setup, shown in Figures 1.3 and 3.1, consists of a magnetron circuit, WR340 waveguide, a Faraday cup to measure the beam current, and solenoid magnets. The magnetron circuit including a magnetron head, a capacitor, and a transformer, is used as the microwave source. It has a 2.45 GHz frequency, 700 W power, and 50 Hz repetition rate. WR340 waveguide, which is suitable to use with 2.45 GHz source frequency, has stub tuners to adjust the impedance of the waveguide. A waveguide system is used to transfer power to oscillate the electrons and to heat up the gas in the plasma chamber. One significant feature of a waveguide is its "mode". The mode determines the electric and magnetic fields across the waveguide's width and height. This setup has TE_{10} (Transverse Electric Field Mode 10), which implies that the electric field has its maximum value in the center of the width of the waveguide. TE_{10} mode is visualized in Figure 3.2. Faraday cup is used to measure the beam current. Electromagnets are used to provide the required magnetic field for the ECR condition in this earlier MDIS system [13].

The electromagnet design of this setup consists of two solenoids, 525 turns each, placed around the plasma chamber. Its cross-sectioned view is visualized using CST simulation software in Figure 3.3, in which the blue arrows stand for the current directions of the solenoids. Magnetic field simulation of this electromagnetic MDIS setup had been conducted using Poisson Superfish simulation software [19]. Its simulation results are shown in Figure 3.4. The field measurements of the electromagnetic setup have been measured using axial magnetic probe through the central axis visualized with blue line in Figure 3.3, the measurement results are given in Figure 3.5 [6, 13].

In this electromagnetic system, solenoids need to be cooled because of the ohmic losses and the plasma chamber's heat. Therefore, the electromagnetic system requires a water cooling setup, which means extra cost and higher maintenance for the project. Also, as the magnets need to be placed around the plasma chamber, they may occa-

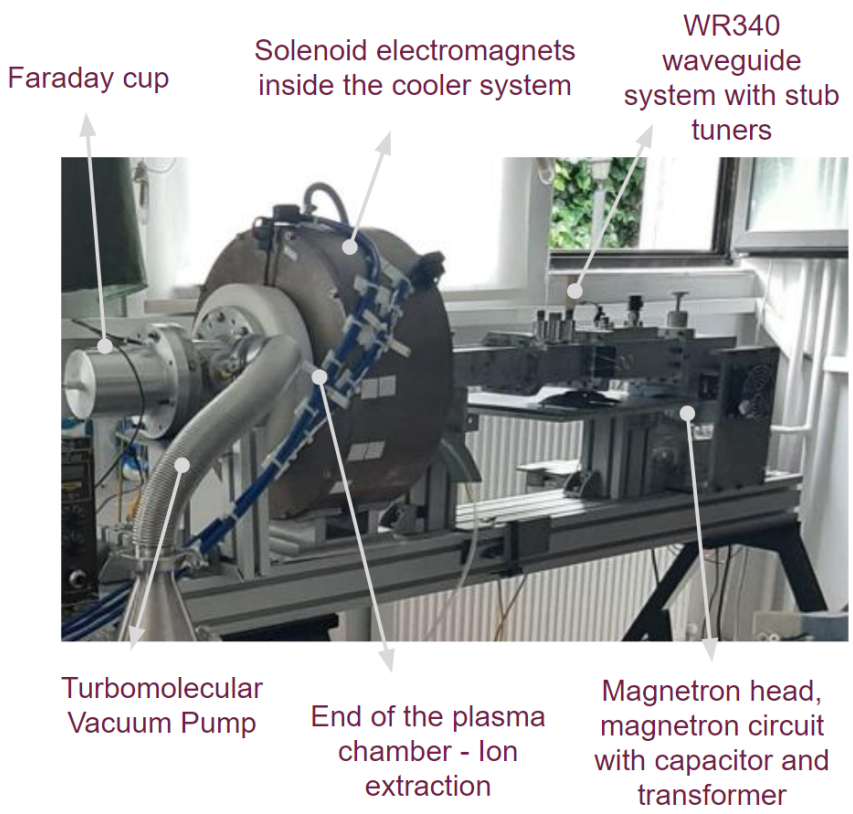

Figure 3.1. Earlier MDIS setup operated with electromagnets.

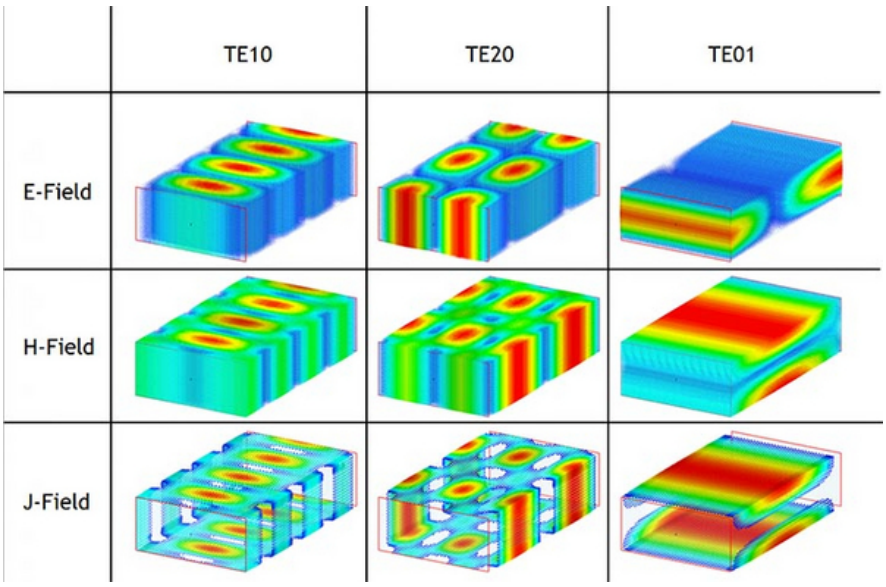

Figure 3.2. Electric (E), magnetic (H), and current density (J) field propagation visualisation for three different transverse electric (TE) modes [18].

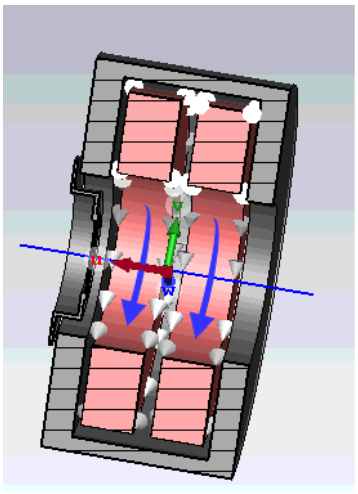

Figure 3.3. Electromagnet design of the earlier MDIS, blue arrows stand for current directions of the solenoids.

sionally cause sparks between solenoids and the plasma chamber. To prevent sparks, either the system needs to be kept under HV, or the insulation material between the plasma chamber and electromagnets is required. In the electromagnetic system, an insulation material, teflon, is used to prevent sparks. However, the insulation material tends to lose its property over time due to the heat.

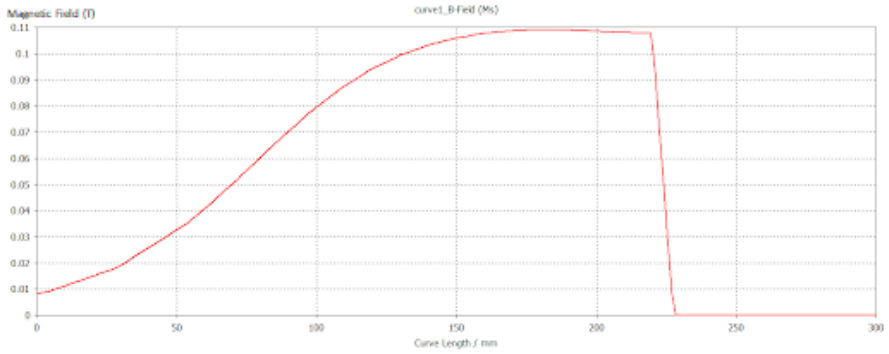

Figure 3.4. Designed magnetic field profile (B_z) of the existing MDIS with electromagnets.

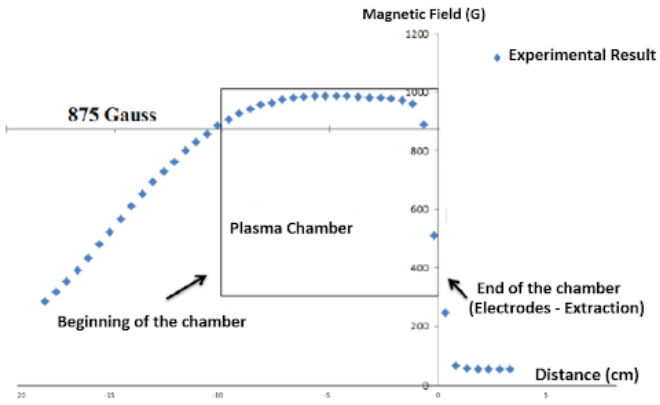

Figure 3.5. The magnetic field measurement (B_z) of the existing MDIS with electromagnets.

3.3. Field Design For The New MDIS with Permanent Magnets

The permanent magnets can be kept under HV and do not require any additional current supply or HV insulation between magnets and the plasma chamber. It is aimed to achieve a more stable and cost-efficient setup by replacing electromagnets with permanent magnets. Taking into account the limitations of and issues regarding the electromagnetic system, it was decided to construct a new MDIS with permanent magnets as an alternative to the electromagnetic system. Required magnetic field to satisfy ECR condition for MDIS will be provided by permanent ring magnets that will be placed around the plasma chamber.

The plasma chamber has a nearly 130 mm outer radius. Such large radius requires powerful magnets to provide the needed 875 Gauss magnetic field throughout the plasma chamber. Therefore, the size of the magnet grows, exceeding the standards, and then it needs to be produced specially abroad. Moreover, transportation of such a powerful magnet is difficult. Due to its size, special production and transportation, it would cost too much. Therefore, instead of special production, it is preferred to design and produce a new permanent ring magnet by combining small, standard sized rectangular magnets. For this purpose, N40 type neodymium magnets (NdFeB) having

1.26 T residual magnetic flux have been chosen because they are easily accessible, powerful, and have many dimension options which provide convenience during the design studies. NdFeB magnets are resistant up to 80°C temperature, but after this limit it is preferred to cool them to prevent any loss in magnetisation.

Many simulation studies have been conducted to optimize magnet configuration and field profile over the chamber. The magnetization direction of the magnets should be in a radial direction to create the magnetic field in the z direction. One of the first trials is shown in Figure 3.7, in which there are two rows each having 16×2 pieces of 20×20×20 mm cubic and horizontally magnetised magnets, shown in Figure 3.6. All of the small magnets have identical radially inward magnetization direction. The simulation results, as a function of the distance between two ring rows, given in Figure 3.8, can not match the requirements.

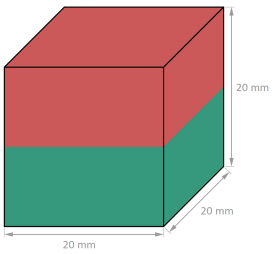

Figure 3.6. A horizontally magnetised, 20×20×20 mm cubic neodymium magnet [20].

To strengthen the magnetic field, we tried to increase the number of magnets and decrease the inner radius, but failed. The most effective way is to decrease the distance between two ring magnet rows. The field profile is still unsatisfactory, and it is not possible to reach the needed 875 Gauss at the extraction point. It was noticed that two rows of magnets should have opposing directions of magnetization to strengthen the field. Actually, this observation seems obvious while working with lengthwise magnetised magnets, which have N and S poles located on the left and right ends. However, for the horizontally magnetised magnets, we needed to simulate and analyze the output. The trial configuration after such direction adjustment is shown in Figure 3.9, its simulation results for B_z direction, given in Figure 3.10, looks similar to the mag-

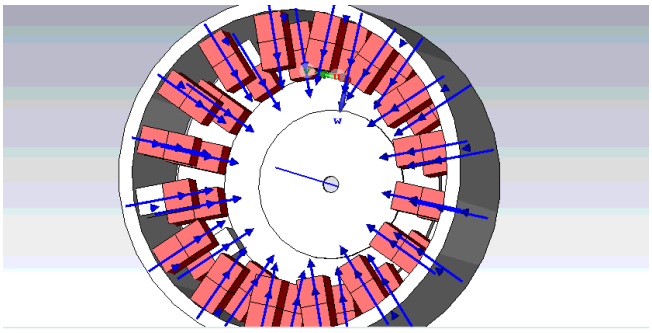

Figure 3.7. One of the first trial designs having 2 rows each having 16×2 pieces of cube magnets, and radially inward magnetization direction. Blue arrows show magnetization direction for each magnet.

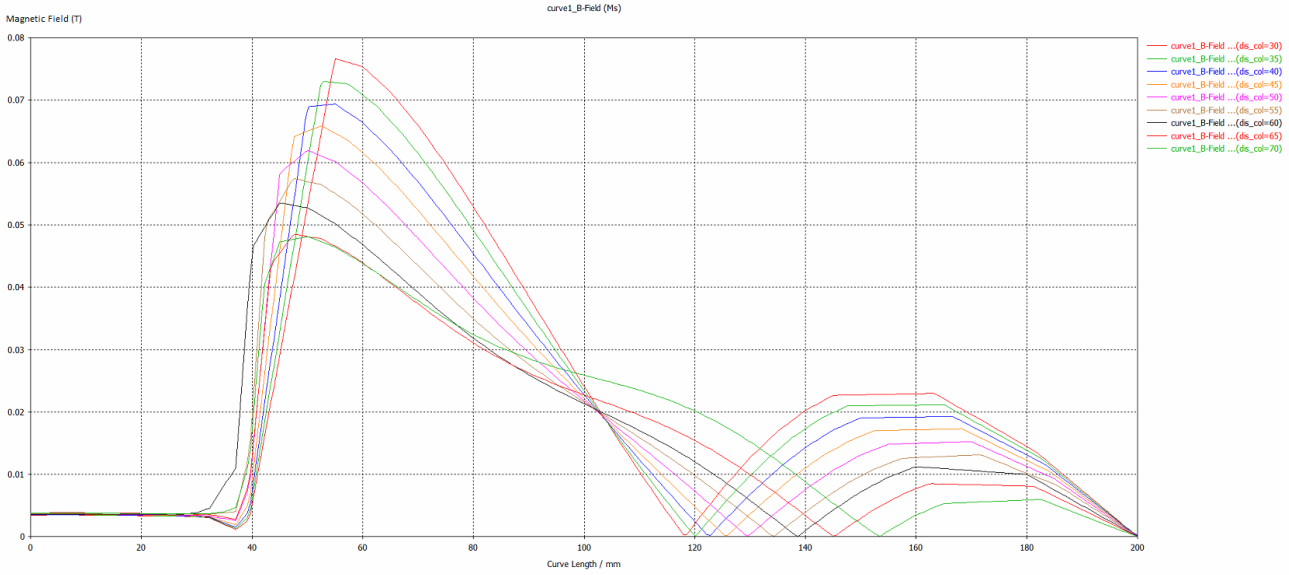

Figure 3.8. CST simulation results (B_z) for the configuration shown in Figure 3.7 for varying seperation between two magnet rows.

netic field profile of the electromagnets. However, it still can not achieve the needed 875 Gauss through the plasma chamber. Further optimization is performed by changing the configuration details such as iron cage thickness, the distance between magnets, magnet count, size, and locations. One of the comparison simulations based on changing distance (20-80 mm) between two magnet rows is given in Figure 3.11.

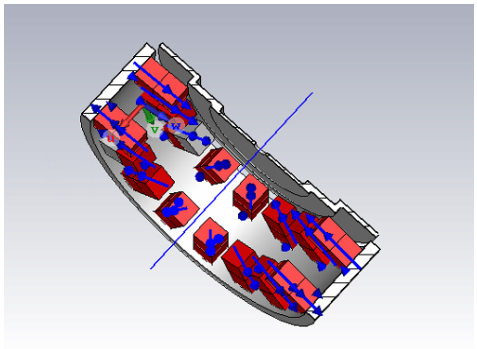

Figure 3.9. Magnet configuration after adjusting magnetization directions.

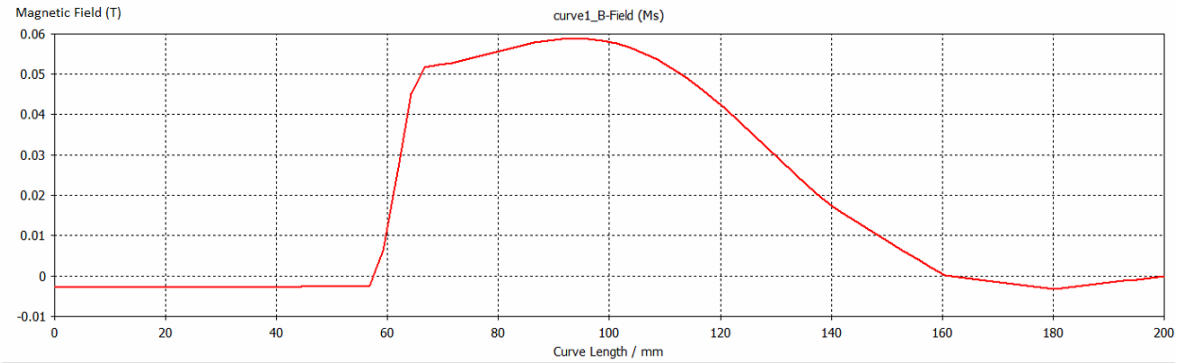

Figure 3.10. Simulation results (B_z) after adjusting magnetization directions.

After many iterative simulation optimizations carried out with the CST simulation software, the magnetic field profile and ring magnet design of the PM-MDIS are completed using 32 N40 type horizontally magnetised neodymium block magnets (two ring magnets, each containing 16 block magnets). The block magnet can be seen in Figure 3.12. The permanent magnet configuration configuration can be seen in Figure 3.13.

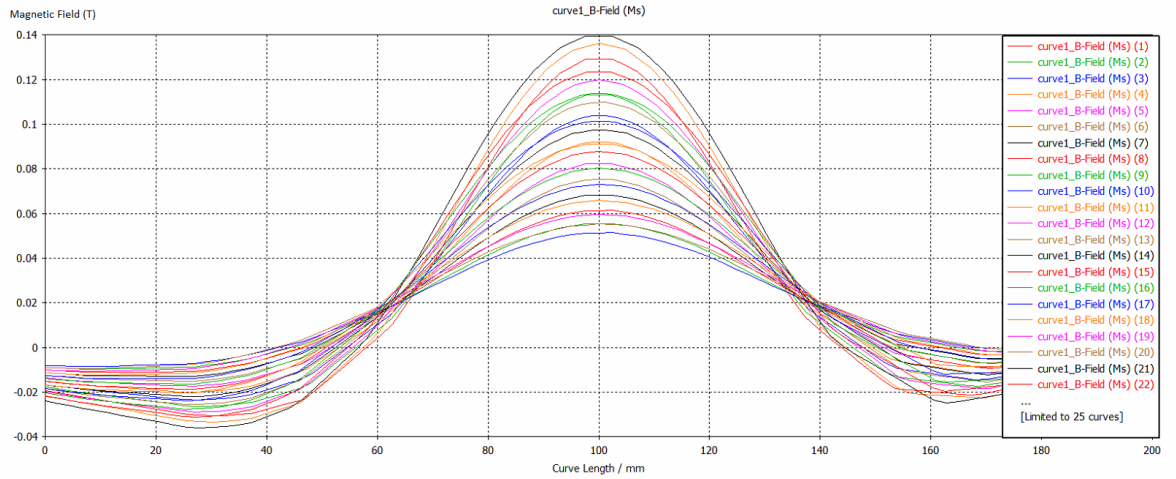

Figure 3.11. Simulations with changing distance (20-80 mm) between two magnet rows. This model does not include the iron cover which reduces field to 0 Gauss at the extraction point.

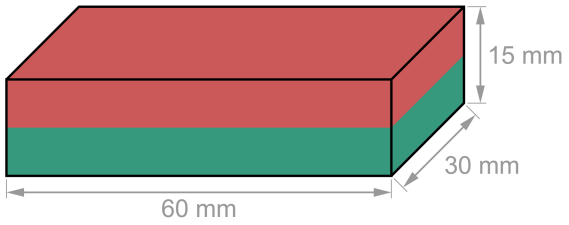

Figure 3.12. A N40 type horizontally magnetised neodymium block magnet [20] .

The designed permanent magnet MDIS system is meant to operate in a similar setup to the electromagnetic one, which is shown in Figure 1.3 and Figure 3.1. In Figure 3.14, the design for the permanent ring magnet and the plasma chamber is presented. Its technical drawings can be seen in Figure 3.15 and Figure 3.16. The ring magnets are placed between an ST-37 type iron cage and an aluminum chamber. The iron cover, having an ion extraction hole at its center, is designed to drop the magnetic field to about 0 Gauss at the end of the plasma chamber. The simulation result for the designed magnetic field of the new PM configuration is given in Figure 3.17, in which the plasma chamber is placed between 60 mm and 165 mm. The magnetic field satisfies

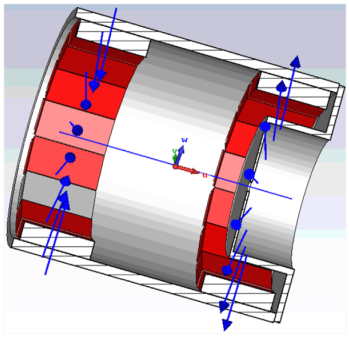

Figure 3.13. Permanent magnet design of the new PM-MDIS, blue arrows show magnetization direction for each neodymium magnet.

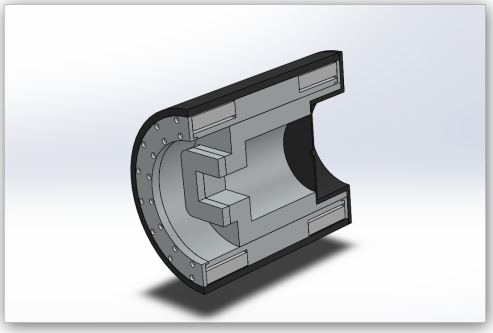

Figure 3.14. Permanent ring magnet and plasma chamber design for MDIS.

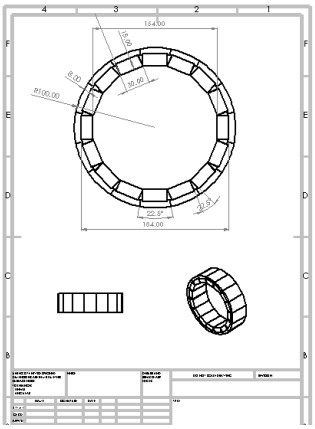

Figure 3.15. Technical cross section drawing for ring magnet on one side.

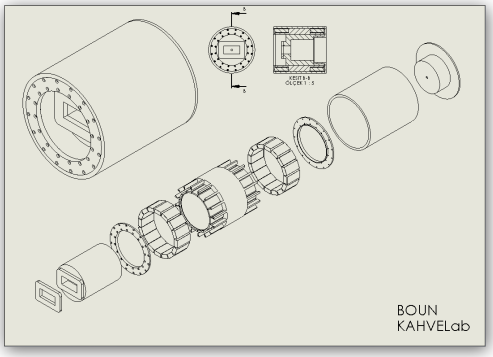

Figure 3.16. Technical drawings of permanent ring magnet and plasma chamber design for MDIS.

820 Gauss at the entrance of the plasma chamber, which corresponds to the vacuum window location at 60 mm, and drops to 0 Gauss at 170 mm, which corresponds to the end of the plasma chamber and electrodes as shown in Figure 3.17. Studies carried out with the CST simulation software shows that the magnetic field design target can be achieved.

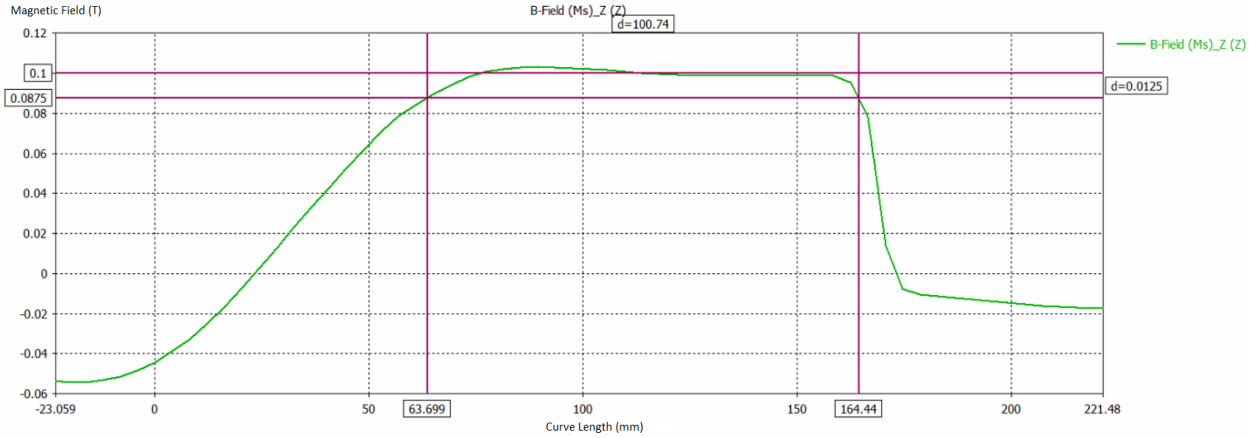

Figure 3.17. The designed magnetic field profile simulation (B_z) of the magnet configuration for new PM-MDIS system.

3.4. Field Measurements On The Single Magnet

Having obtained a viable design, the 60×30×15 mm block magnets with approximately 549 N strength have been purchased from a German company [20]. The measurement setup, needed to compare the claimed magnetic field value on the surface with the simulations to confirm the accuracy, is shown in Figure 3.18.

Field measurements have been performed four times as shown in Figure 3.19. The comparison plot for the CST simulation results and the mean value of the measurements are given in Figure 3.20. As it can be seen, measurement and simulation results do not appear compatible at the boundaries.

Figure 3.18. Field measurement setup with single magnet.

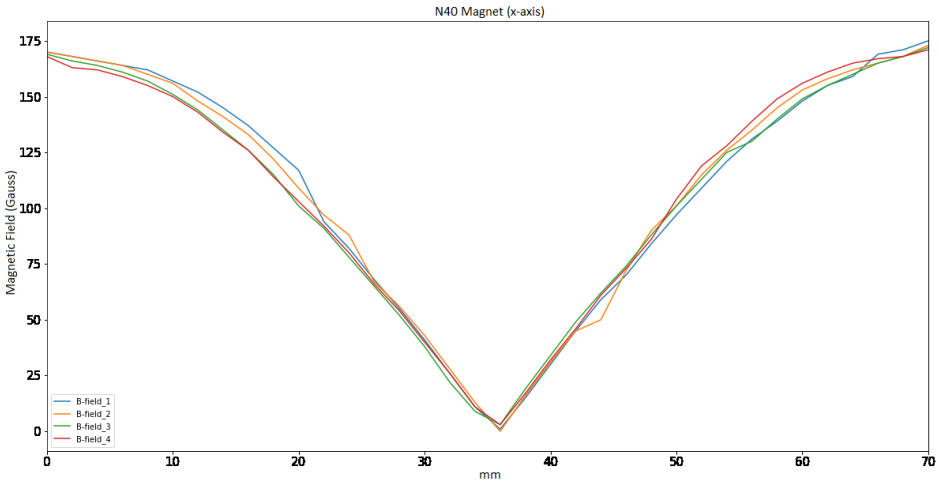

Figure 3.19. Measurement results for the single magnet field test setup.

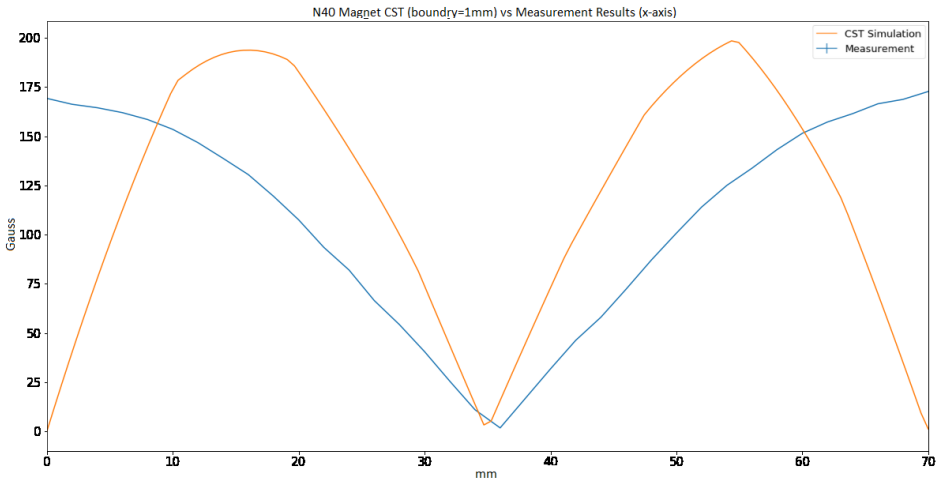

Figure 3.20. CST field simulation vs measurement comparison plot for the test setup designed with single magnet.

While conducting simulation studies, proper selection of the volume surrounding the model to be simulated, is critical. In particular, in the simulation studies conducted in open borders such as this experiment, simulations should be run with the widest possible volume boundaries. To visualize the effect of the boundaries, multiple simple simulations were conducted with the boundary values between 20 mm to 70 mm. The results are given in Figure 3.21.

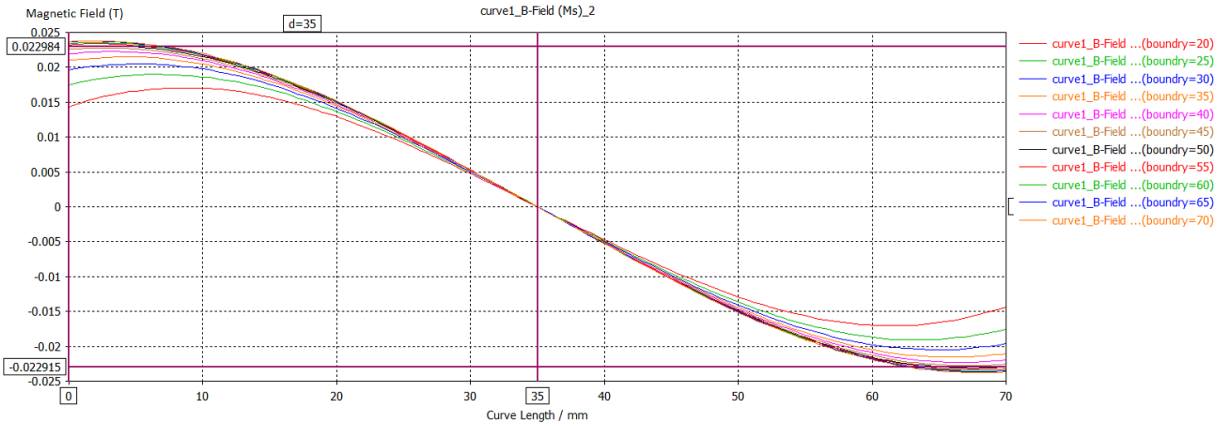

Figure 3.21. Repetitive CST simulations with the boundary values between 20 mm to 70 mm to visualize the effect of the boundry setting.

For this test experiment on the surface of a single magnet, the maximum boundary value is 50 mm as we are using the student edition of the CST simulation software, which restricts maximum mesh size. We conducted our simulations at approximately 700,000 mesh size. The comparison result for the maximum simulation boundaries is given in Figure 3.22.

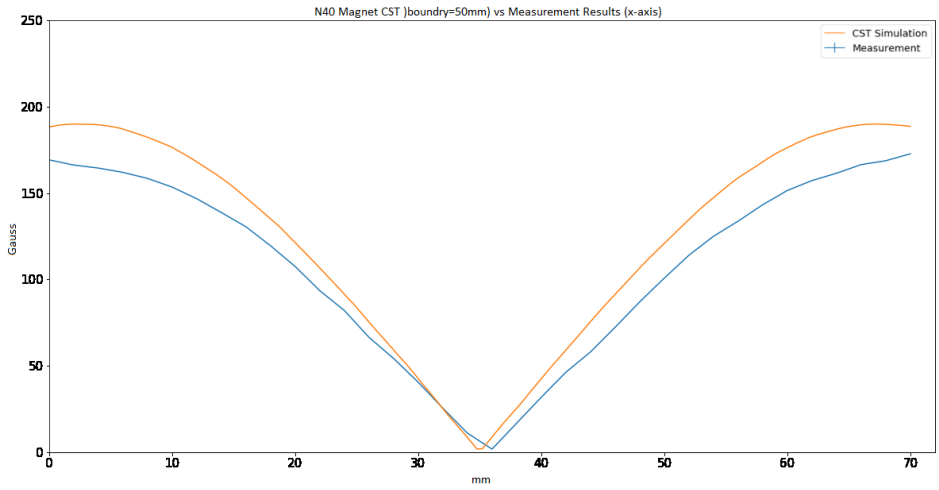

Figure 3.22. CST field simulation at 50 mm boundary vs measurement comparison plot for the test setup designed with single magnet.

Because of the uncertainty in comparisons with open boundaries, it has been decided to design a closed boundary test setup.

3.5. Test Setup Design Including Two Magnets and Its Measurements

Before producing the entire MDIS magnet system, a closed boundary test setup has been designed, including two magnets to ensure consistency between simulation results and measurements. Therefore, it is aimed to investigate whether the simulation results require any calibration.

Test setup includes two magnets placed against each other with a certain separation between them. This setup and its CST simulation can be seen in Figures 3.23 and 3.24. The radial magnetic field in the x-direction is measured along the z-axis using a radial

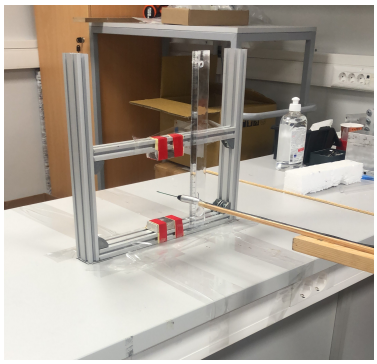

Figure 3.23. Test setup including two magnets.

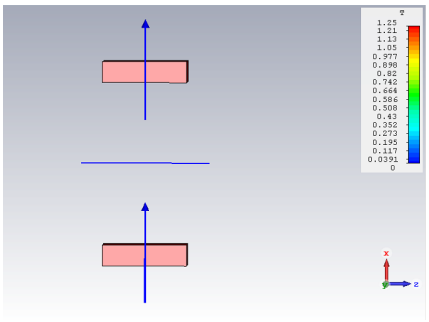

Figure 3.24. CST simulation for two-magnets test setup.

magnetic field probe, and the results are compared with the CST simulation results. Field measurements have been repeated three times, shown in Figure 3.25, to calculate the standard deviation. The mean and standard deviation values are used to plot a comparison between the measurement and simulation results, as seen in Figure 3.26. Standard deviation values of the measurements are plotted as uncertainty bars on the blue line, which represents the mean values for the measurements in the figure. The relative difference between CST simulation and measurement is visualized in Figure 3.27.

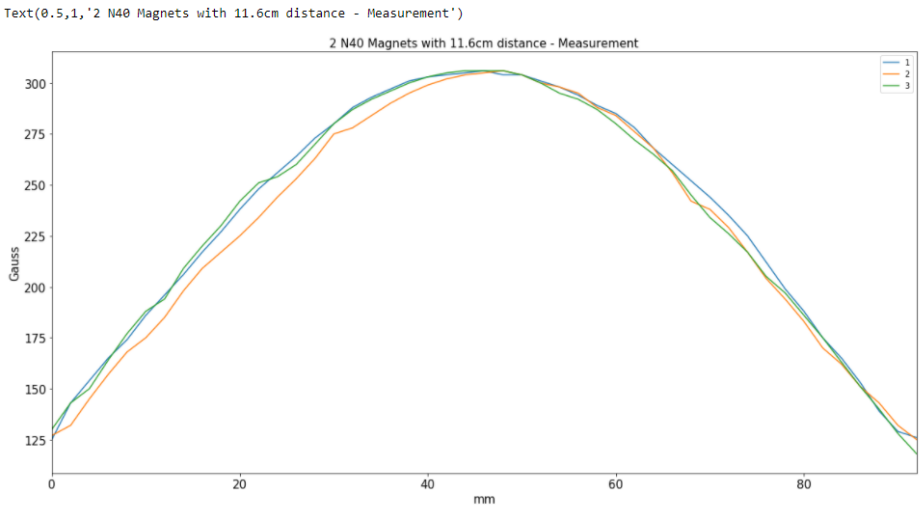

Figure 3.25. Field measurements of the test setup designed with two magnets.

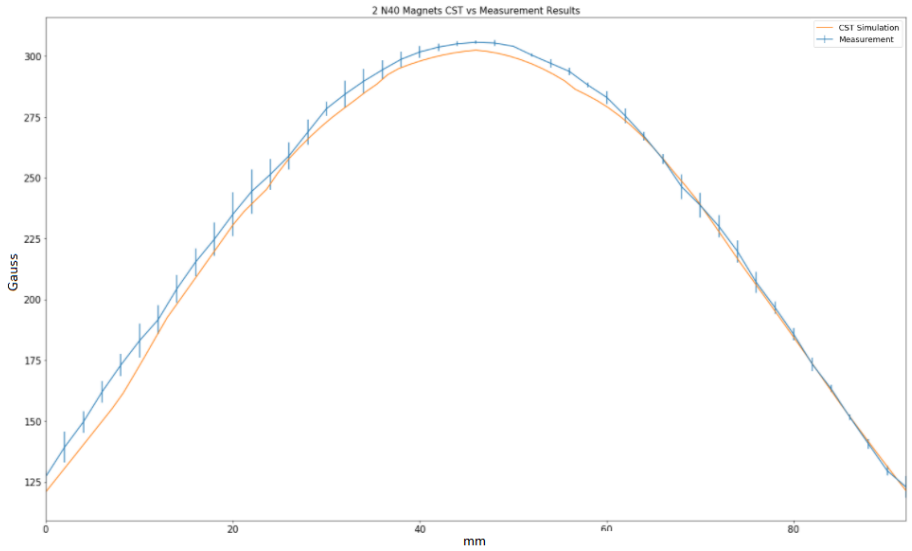

Figure 3.26. CST field simulation vs measurement comparison plot for the test setup designed with two magnets.

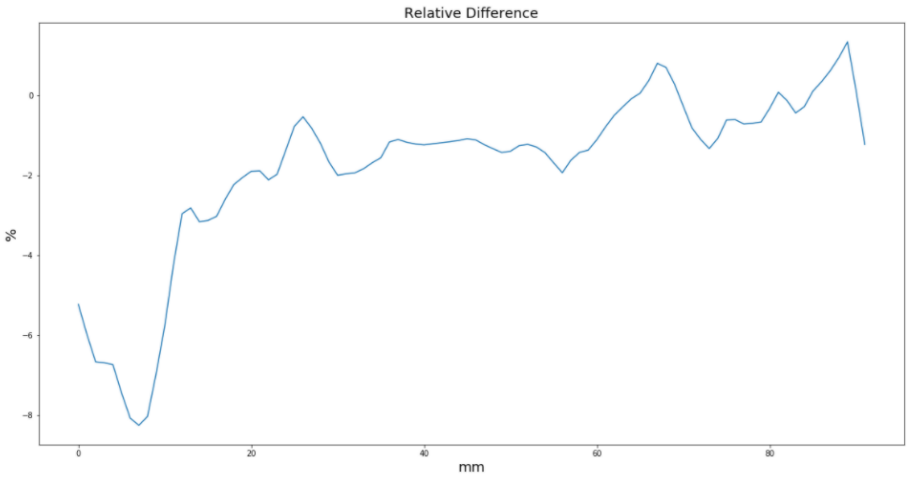

Figure 3.27. The relative difference plot to visualize the difference between CST simulation and measurement results for the test setup designed with two magnets.

As a result of this experiment, it is found that the simulation and measurement results vary up to 8%. The main reason for the error is the problems experienced in fixing the probe when measuring in the first trial setup. In addition, the error margin of the magnetic measuring instrument in the relevant measuring range is 1%. Since the standard deviation of the measurements practically covers this relative difference, the studies have proceeded without any calibration. This result shows that the simulation and measurement are consistent.

3.6. Prototype Construction and Its Measurements

Magnetism is not adjustable for permanent magnets unlike electromagnets. However, by changing the distance between small magnets, the magnetic field can be optimized to some extent. The aluminum case on which the magnets will be placed is designed as three pieces to bring adjustability to the PM setup. Cross section view of this design can be seen in Figure 3.28 in which aluminum components are represented by yellow, ST-37 material is represented by grey, insulator material is represented by white, and permanent magnets are represented by blue color.

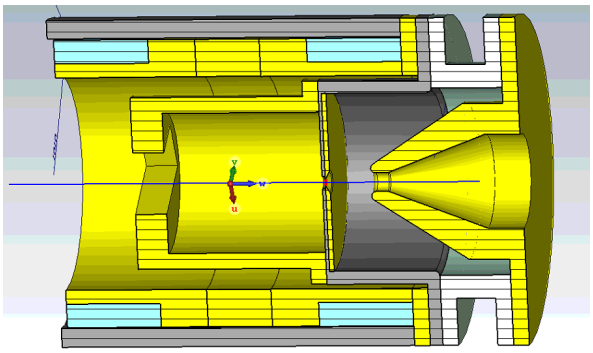

Figure 3.28. The PM-MDIS design with plasma chamber and electrode extraction part.

The successful field test using two magnets, has been proceeded with another trial production before the complete production of the PM-MDIS. Due to the high cost of full fabrication, a secure approach to obtain an accurate result is preferred. One piece

of the aluminum casing and its ST-37 cage is used to assemble one of the dual ring magnet structures in the ion source. This trial production also allows us to determine quality and identify possible defects in advance.

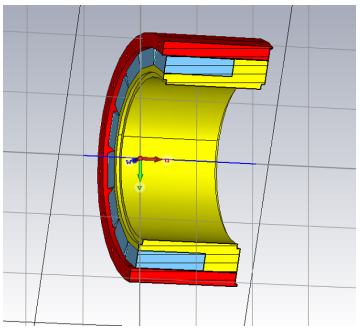

Figure 3.29. The cross sectional view of the trial production which is designed as one of the ring-like magnet assemblies.

Figure 3.29 shows the cross sectional view of this trial production, which constitutes about half of the entire PM design of the ion source. The produced component is shown in Figure 3.30, before and after the permanent magnets are placed. The magnetic field is measured in the radial direction on the central horizontal axis (the line passing through the center axis in Figure 3.29) of the magnets placed inside the ST-37 iron to perform the field analysis. The measurement setup is shown in Figures 3.31 and 3.32. The field measurement process has been repeated three times, mean and standard deviation values have been used to plot a comparison between the measurement and simulation. The measurement results are plotted in Figure 3.33, the comparison is visualized in Figure 3.34, and the relative difference between CST simulation and measurement is visualized in Figure 3.35 using Python Matplotlib library [21].

In this analysis, the difference between the results has been observed as 5% at most and 2% on average. This observation was deemed satisfactory to start the production of the complete ion source. Moreover, as the simulation is compatible with the measurement results, the ion extraction system was also designed using the magnetic

Figure 3.30. The produced trial component before and after the permanent magnets are placed.

Figure 3.31. The field measurement setup for the trial production.

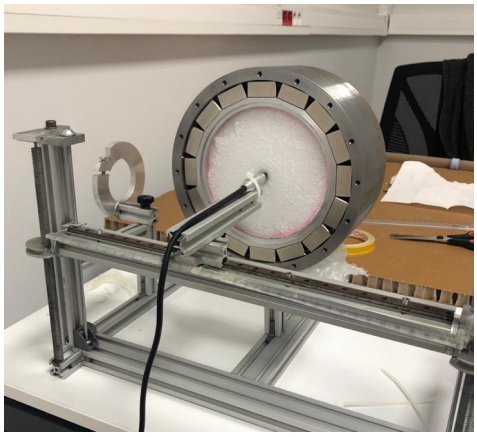

Figure 3.32. Front view of the field measurement setup for the trial production.

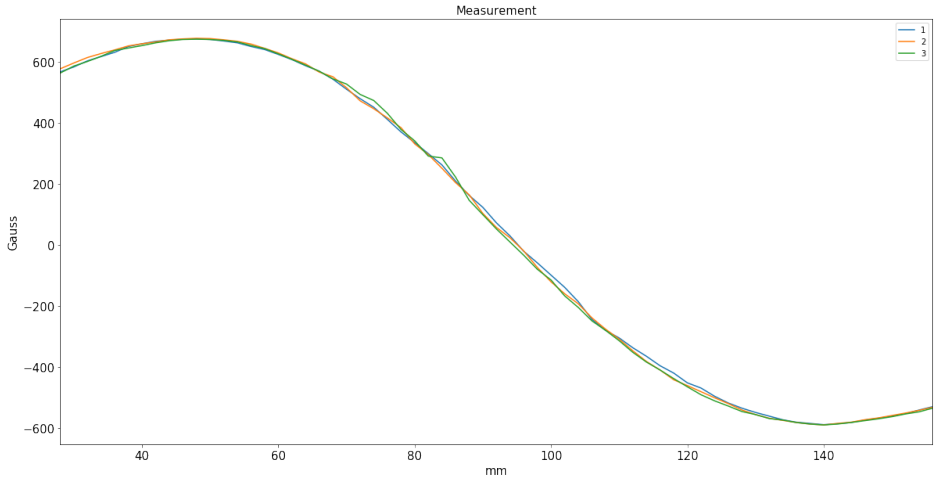

Figure 3.33. Magnetic field measurements with the trial production.

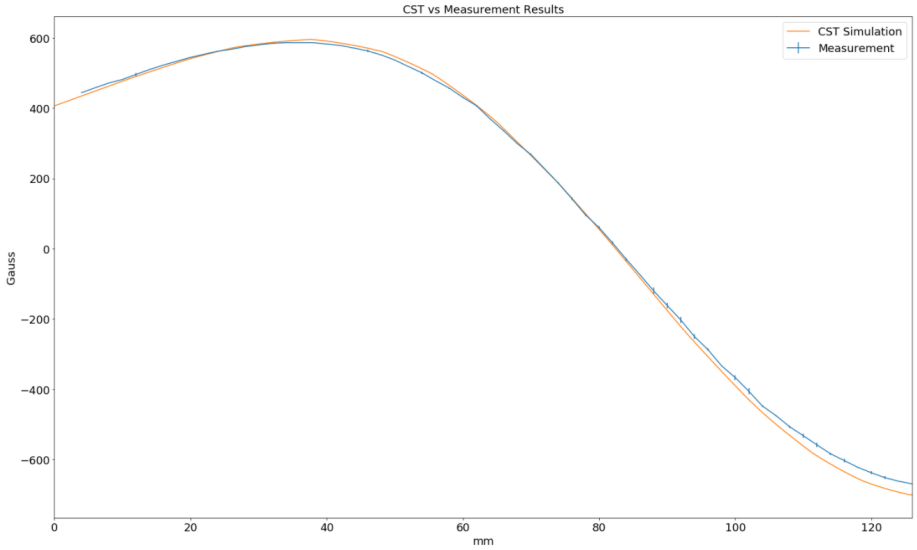

Figure 3.34. CST field simulation vs average measurements comparison plot for the trial production.

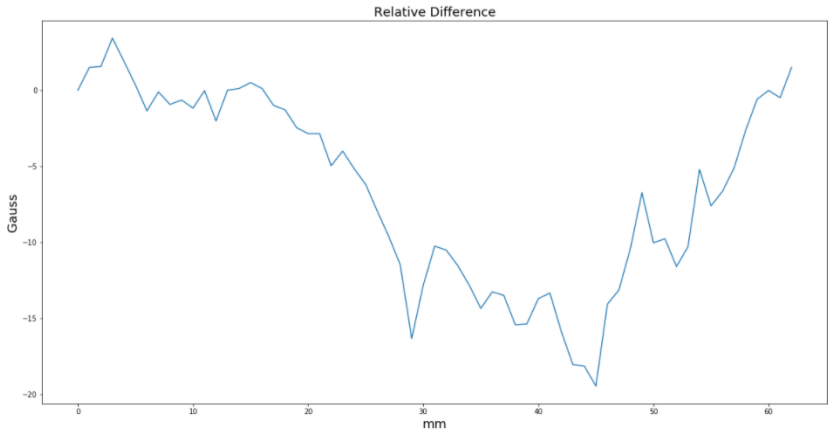

Figure 3.35. The relative difference plot to visualize the difference between CST simulation and measurement results for the trial production.

field data from the simulation results. The ion extraction system design details will be discussed in Chapter 4. The design has been reviewed by a mechanical engineer in our laboratory, including PM-MDIS and the ion extraction unit, and he prepared technical details for the production. Figure 3.37 and Figure 3.36 are the technical drawings sent to the manufacturer.

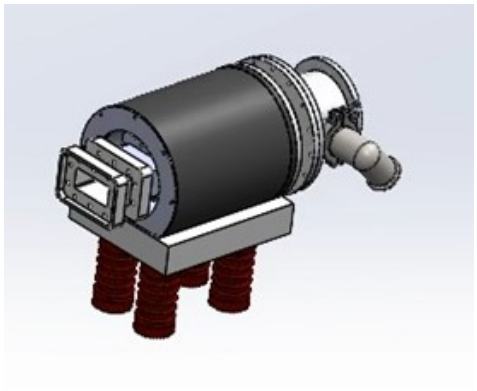

Figure 3.36. The technical drawing for the PM-MDIS design in assembled view.

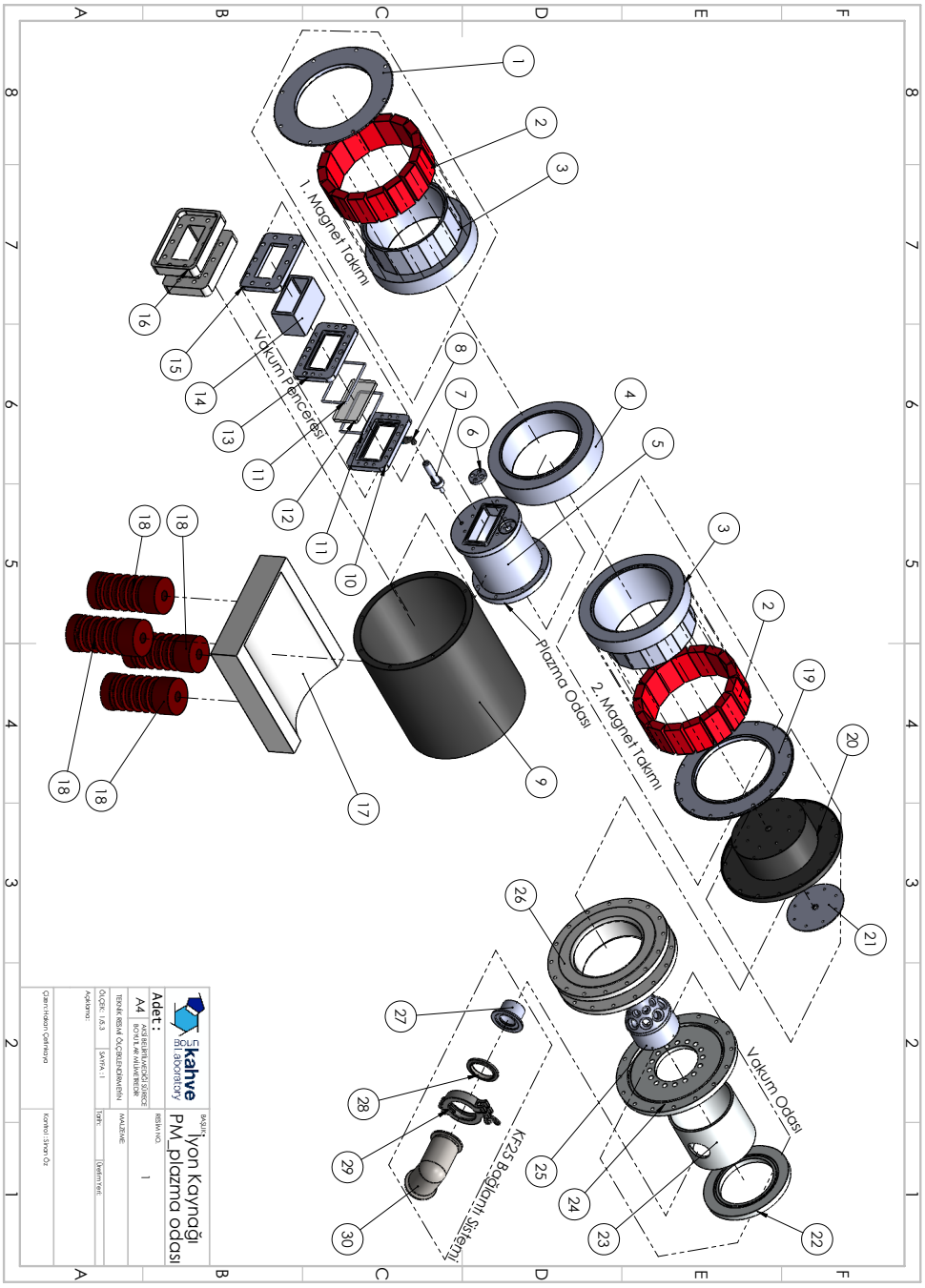

Figure 3.37. Technical drawing in exploded view showing in detail all the parts in the new PM-MDIS design.

3.7. Full Construction and Its Measurements

After the prototype production results were found to be compatible with the simulation results, a company in Ankara was contracted for the entire production of the ion source. In Figure 3.38 all the PM-MDIS components, including the plasma chamber and the dual-electrode extraction system, are shown before assembly.

Figure 3.38. The PM-MDIS components, including the plasma chamber and the dual electrode extraction system are shown before assembly.

As a first step, N40 type neodymium permanent magnets with strong magnetic field have been placed between the aluminum part and the ST37 iron so that they do not move. Figure 3.39 shows the state after permanent magnets are placed between the aluminum part and the ST37 iron. Figure 3.40 shows the produced plasma chamber including its vacuum window and the gas entrance pipe. The fused quartz silica vacuum window [22] allows wave propagation of microwave from air to vacuum medium and it is also used as vacuum break.

Figure 3.39. The system after the permanent magnets are placed between the aluminum part and the ST37 iron.

Figure 3.40. Produced plasma chamber including vacuum window and gas entrance pipe.

3.7.1. PM-MDIS Magnetic Field Measurements

After 32 permanent magnets have been placed on the iron surface in 2 rows, the system's magnetic field is measured to make a comparison analysis with the simulation results. In Figure 3.41, the blue line shows the axis on which the magnetic field calculations are performed. In Figure 3.42, the magnetic field measurement setup is shown from two different angles.

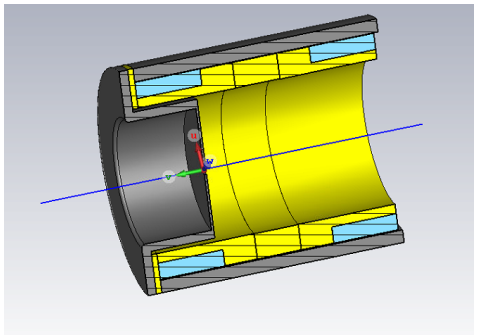

Figure 3.41. The CST visualization of the system with permanent magnets which are placed between aluminum casing and ST-37 iron cage.

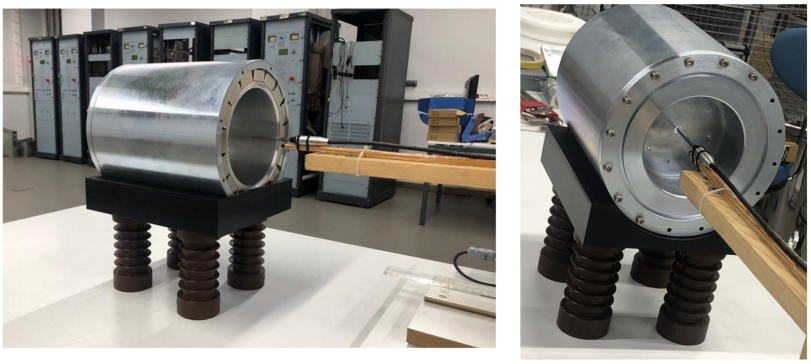

Figure 3.42. The field measurement setup from two different angles.

The measurement process has been repeated three times. The mean and standard deviation values have been used to plot the comparison between the measurement and simulation. The CST simulation results are shown in Figure 3.17, the measurement

results are given in Figure 3.43, their comparison is visualized in Figure 3.44 in which the red horizontal line shows the ECR condition value of 875 Gauss, and the relative difference between CST simulation and measurement is visualized in Figure 3.45.

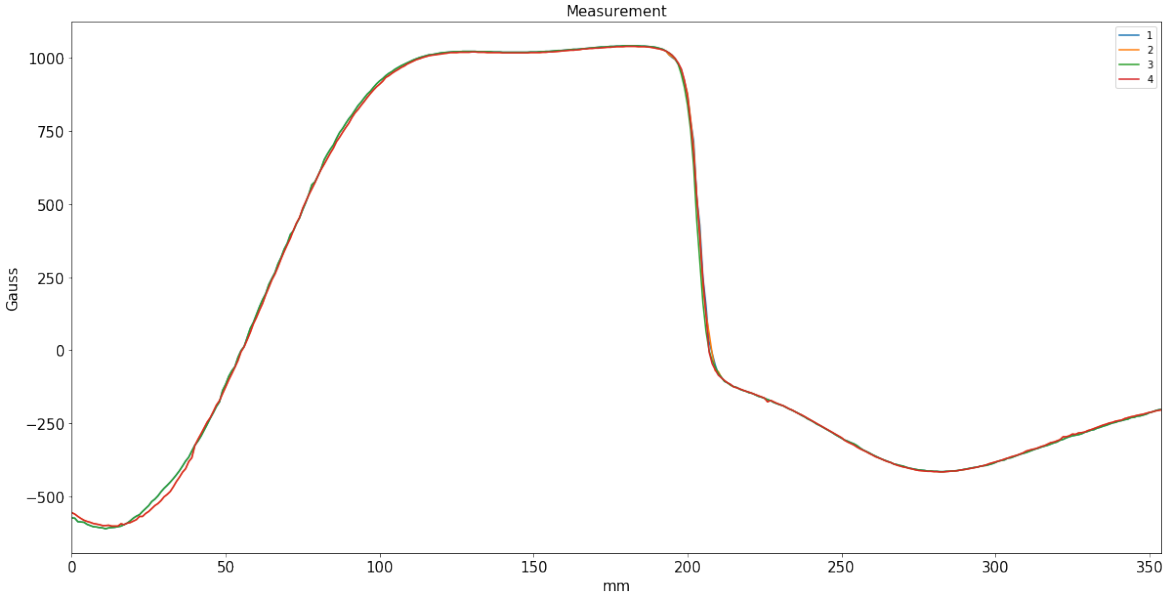

Figure 3.43. Full production field measurements.

In this analysis, it is observed that the relative difference between the results is ∼4% at most and ∼2% on average in the region over the chamber. The relatively higher errors encountered in previous measurements are reduced by making the probe attachment setup more stable. The margin of error in the measuring probe may have affected the results here as a systematic error. Also, restrictions in mesh size can cause this error. Normally, it is expected that the aluminum material is magnetically permeable. However, as it has been observed after production, the aluminum has become somewhat magnetised, probably because of the metal dust contamination during the production. Additionally, the margin of error due to the production of the magnet and the difference due to the components in the production of the ST37 material, all of these have an effect on the margin of error and cause the error to come out irregularly. Overall, the results are observed to be satisfactory for proceeding with the rest of the project.

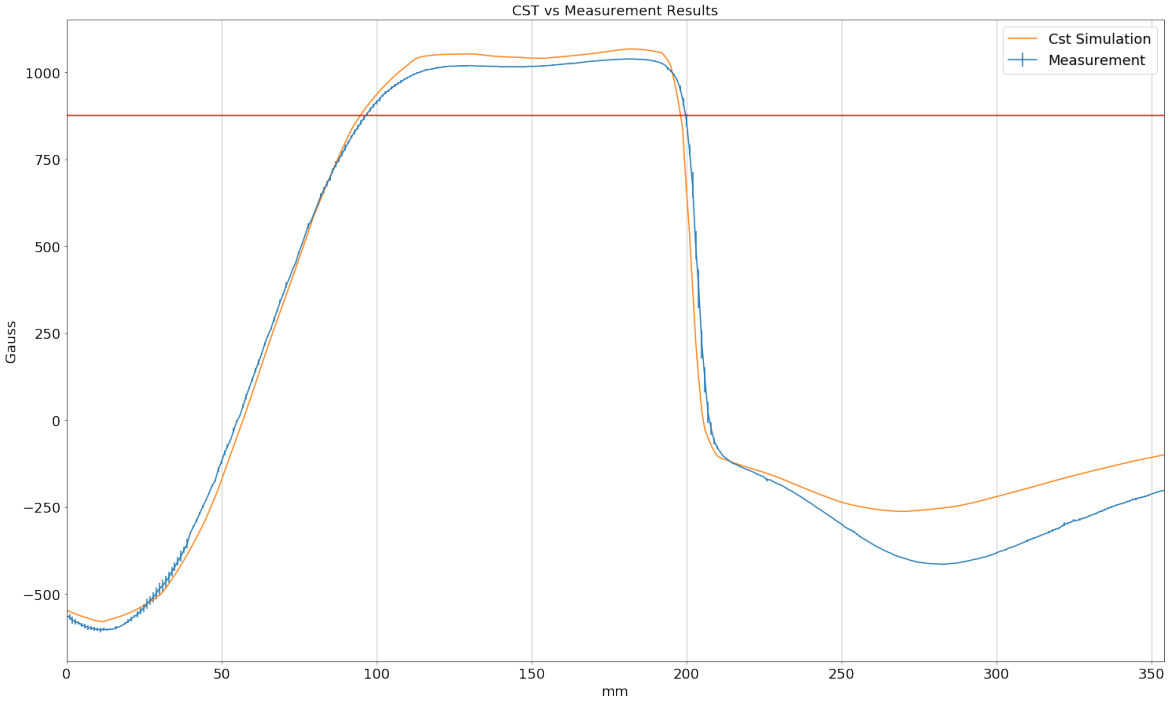

Figure 3.44. CST field simulation vs measurement comparison plot for the full production, red line shows ECR condition value 875 Gauss.

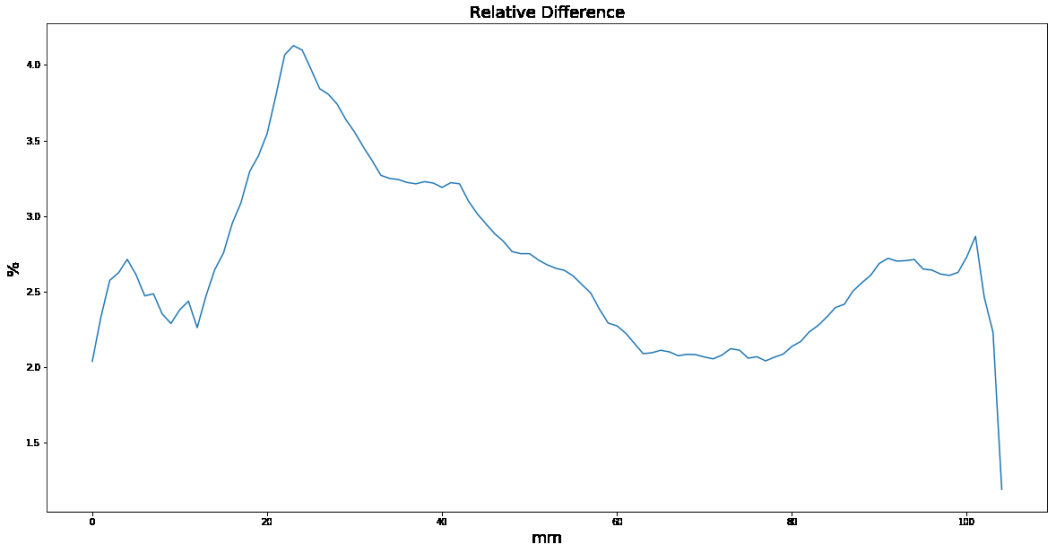

Figure 3.45. The relative difference plot to visualize the difference between CST simulation and measurement results for the full production.

4. ION EXTRACTION UNIT

An ion extraction unit is required to draw and form the proton beam to be transferred to the beamline from the ion source at the desired current, energy, and emittance. An ion extraction system is composed of two or more electrodes fed with high voltage. Electrodes can be designed in many different geometries according to the system requirements. In Figure 4.1, a scheme for the simplest extraction unit is illustrated.

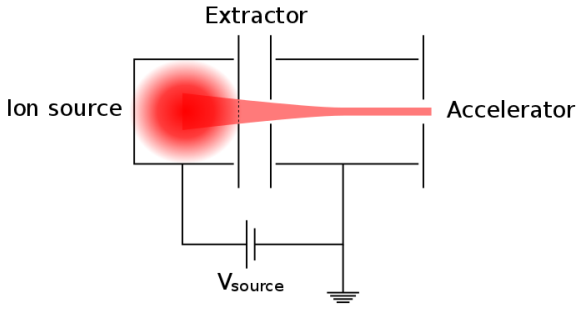

Figure 4.1. A general scheme for the simplest extraction unit [23].

A simple extraction system consists of a plasma electrode at potential V and a ground electrode. In this case, a particle, with charge q, to be extracted using plasma electrode at potential V from the ion source, will have the initial energy $E = q\Delta V$. The plasma electrode is usually kept at the same potential with the plasma chamber to prevent electrical discharge instability. The potential difference between electrodes is determined according to the system requirements.

4.1. Design Constraints

An ion extraction system should satisfy the following requirements to extract beams suitable for the beam line. The desired beam current for the beamline should be taken into consideration while designing an electrode extraction unit for the ion source. The target beam current is about 1 mA for this study. Also, extracted proton

beams to be transferred to the RFQ cavity from the MDIS need to satisfy a matching emittance value at the entrance to the RFQ.

4.1.1. Electrode Geometry

4.1.1.1. Pierce Angle. Space charge forces try to spread the incoming beam. This phenomenon usually occurs in the initial acceleration interval due to the low velocity of the particle in the beam. The shape of the electric field in the acceleration cavity shapes the beam transferred to the beamline [13]. The electrodes can be shaped in such a way that if the electric field in the first acceleration cavity focuses the particles in addition to accelerating them, the beam scattering problem is held in check. Considering the electrons emitted from the surface, there is a solution for this situation. In this solution, the shape of the electrode at the cathode is designed to make an angle of 67.5° with respect to the emitting surface normal axis, which is known as Pierce geometry and illustrated in Figure 4.2.

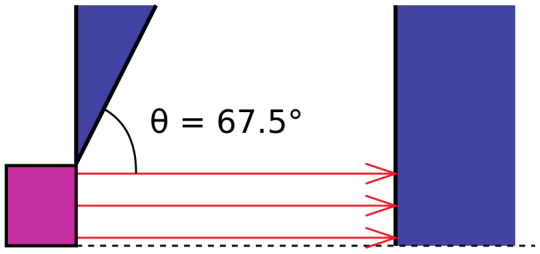

Figure 4.2. Parallel extraction of surface emission electrons using the Pierce geometry [2].

In plasma ion sources, completely parallel beam focusing is not possible because ions do not start from a stable surface, but from a plasma medium with varying initial conditions [2].

4.1.1.2. Corona Discharge. Corona discharge is a type of partial discharge. It is likely to occur at fields near a sharp point which causes the electric field lines to become

stronger and make a very localized high-field region. This phenomenon is shown in Figure 4.3 [2]. To prevent corona discharges from sharp points, soft curves should be added to those tips.

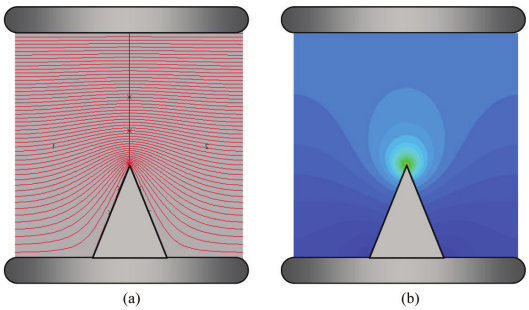

Figure 4.3. (a) Equipotential lines and (b) electric field strength around a point [2].

4.1.2. Vacuum

The breakdown voltage (electrical discharge) of a gas between two parallel plate electrodes depends on the electron mean free path and the distance between the electrodes [2]. The mean free path is the average path a particle can take before it collides with another atom. It is directly related with pressure.

In 1880, Friedrich Paschen investigated the breakdown in gases and found a relation between breakdown voltage (V_b), pressure (P), and the distance between the electrodes (d), which is written as

$$V_b = \frac{aPd}{\ln Pd + b} \tag{4.1}$$

where a and b are the gas-dependent constants [2]. The graph of this function is called the Paschen curve. From this graph, the minimum voltage required for the electrical breakdown of each gas can be determined. A Paschen graph for a few gases is given in Figure 4.2. It should be taken into consideration while designing an electrode.

High pressure means short mean free path. Therefore, a particle can not take enough path to be accelerated before colliding with another particle. At very low

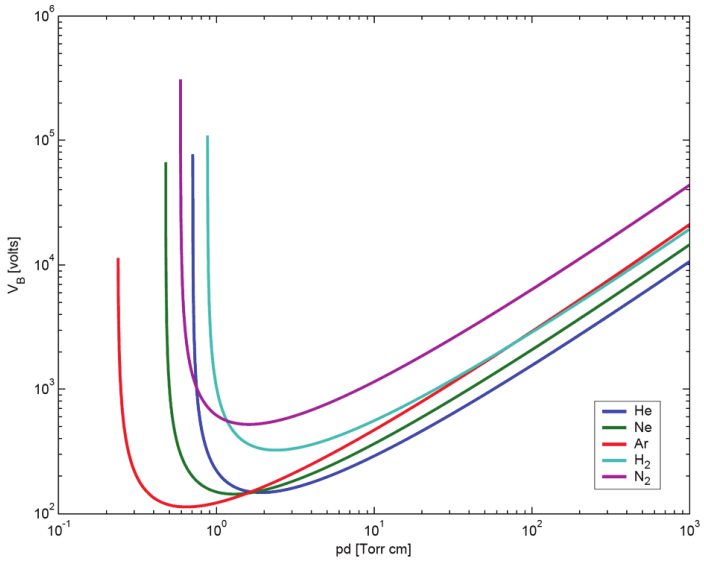

Figure 4.4. Paschen curves for various gases [2].

pressures, the mean free path becomes long enough not to collide with any particle and get accelerated to the desired energy. Vacuum is used essentially as an insulating medium to increase the mean free path.

4.1.3. Distance Between The Electrodes

The distance between the plasma and ground electrodes affects the maximum field strength. While determining the separation between any two electrodes, it should be determined and designed theoretically in accordance with the voltage to be applied. Kilpatrick has shown the relation between the applied maximum voltage and the distance between the plates as

$$U_K = \frac{1.8 \times 10^{18}}{E^2} e^{\frac{1.7 \times 10^7}{E}} \sim 1.7 \times 10^6 d^{2/3} \tag{4.2}$$

where U is the applied potential difference in volts, d is the distance between electrodes in meters, and E is the electric field strength in volts per meter [24].

Another relation was found by Coupland [8, 25], which is expressed as

$$U_C = 6 \times 10^5 \sqrt{d}. \tag{4.3}$$

In Figure 4.5, the extractable ion beam current is given as a function of the aspect ratio for Coupland's and Kilpatrick's law. Aspect ratio is defined as $S = r/d$ where r is the electrode aperture radius and d is the distance between electrodes.

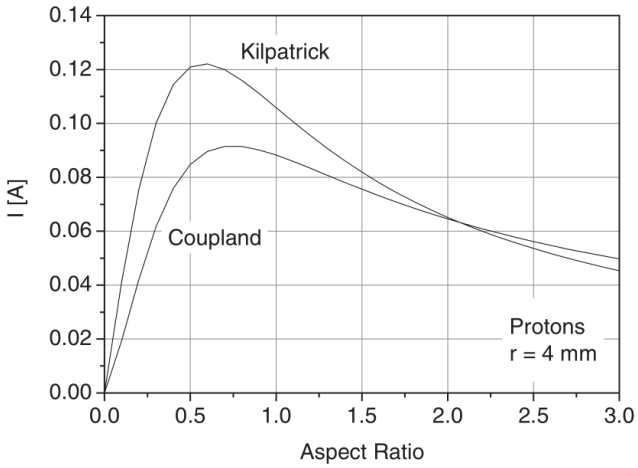

Figure 4.5. Extractable ion beam current is given as a function of the aspect ratio for Coupland's and Kilpatrick's law at constant electrode aperture radius $r = 4\,\text{mm}$ [8].

4.1.4. Emittance

In accelerator physics, emittance is a property of a charged particle beam. It is a measure of the area occupied by the beam in a position and momentum phase space [26]. To transfer extracted proton beams from the MDIS to the RFQ cavity, the normalized emittance value should be at most $0.2\,\pi$.mm.mrad at the entrance to the RFQ [4].

4.2. 20 kV Dual-Electrode Extraction Unit and Its LEBT Configuration

To extract ions from hydrogen plasma, a dual-electrode system consisting of plasma and ground electrodes has been designed in accordance with the magnetic field profile of the new PM-MDIS system. The distance between the plates of the dual-electrode is calculated according to the theoretical equations, as it may cause sparks when they are close to each other or decrease in field strength between these

electrodes. Two different equations are used while calculating this distance between plates to optimize voltage limit and distance parameters; the Coupland's equation [25], and the Kilpatrick's equation [24]. Also, other constraints from Section 4.1, have been taken into account.

PM-MDIS beam extraction simulations have been carried out using IBSIMU [27] program, as integrated into the DemirciPro [28] software. IBSIMU is a simulation software package for ion extraction and space charge dominated ion beam transportation optics, Vlasov iteration using finite difference method (FDM) [27]. DemirciPro is a light ion RFQ beamline designer software written in C++ using ROOT [29]. It supports ion source (with IBSimu integration), LEBT, and beam properties measurement box simulations using the three-dimensional finite element method (FEM) [28]. LEBT line configuration simulation studies have been carried out using DemirciPro.

Simulation studies have been carried out at changing current densities by applying a potential difference of 20 kV between the electrodes. During the electrode design studies, it is aimed to transfer the proton beam to the LEBT line with an emittance value of less than $0.2\,\pi$.mm.mrad, without hitting any electrode, and having a beam current of about 1 mA. To minimize the corona discharge effect which is mentioned in Section 4.1.1.2, arc curves have been added to the sharp edges. The ground electrode is designed as an inclined shape to protect against electrical jumps between the two electrodes, as well as the corona discharge effect. Also, it has vents on the inclined surface to increase the vacuuming efficiency. The design of the plasma and ground electrodes can be seen in Figure 4.6.

In KAHVELab, there is an existing LEBT line which is used to transfer the proton beams from the extraction point of the ion source to the RFQ cavity to transfer most efficiently. It has been designed using Travel [30] and DemirciPRO [28] softwares. The LEBT line has a 1.53 m length and it was previously designed, produced, and configured for the electromagnetic microwave ion source setup. This LEBT line, which can be seen in Figure 1.1, includes two solenoids, two steerer electromagnets, and Measurement Box (MBOX) between them. In this LEBT system, electromagnets are

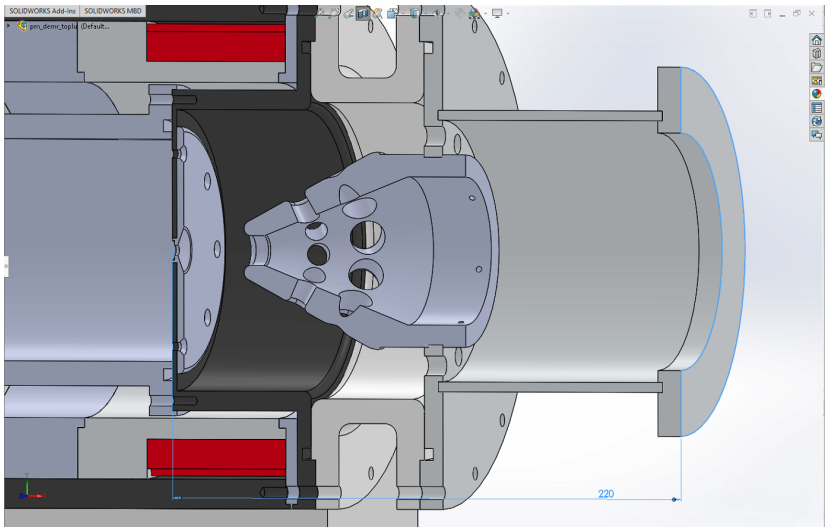

Figure 4.6. Electrode extraction unit design, which consists of a flat plasma electrode and an inclined ground electrode.

used for focusing, defocusing, and steering the beam. The MBOX design includes a Faraday cup to measure current, a pepper pot plate to measure emittance, and a home-built scintillator screen to monitor the profile of the incoming beam. The MBOX has been designed to ensure required beam property matching between MDIS and RFQ input. The measurement apparatuses inside the box are controlled from outside with three pneumatic cylinders [31].

The LEBT line has been reconfigured in accordance with the new ion source properties in this PM-MDIS study. This configuration aims to reduce paricle loss and optimize the normalized emittance by adjusting the magnetic field profile through the beam pipe via solenoids. In Figure 4.7, simulation results of the electrode system and the beam trajectory in the LEBT line can be seen. A 1.3 mA beam at the end of the LEBT line can be achieved without loss. After completing its design and simulation studies, the electrodes have been produced by a local computer numerical control (CNC) manufacturing company. The produced ground electrode can be seen in Figure 4.8. In Figure 4.9, the final configuration of the LEBT line is given.

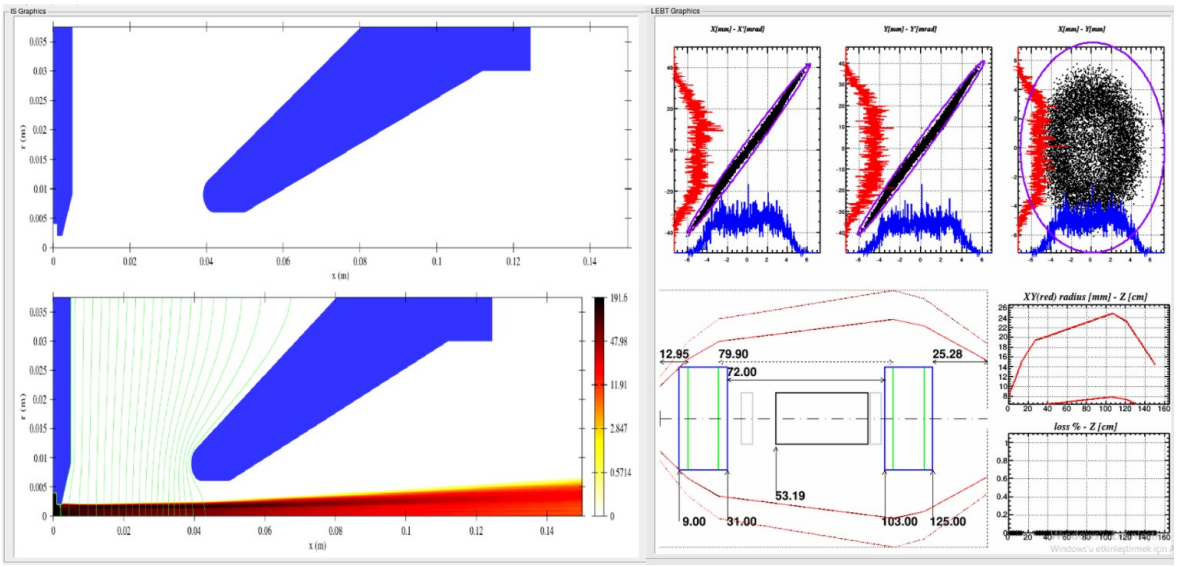

Figure 4.7. Beam diagnostics for H^+ ions with DemirciPro Software. Current density $= 180\,\mathrm{A/m^2}$, beam current $= 1.3\,\mathrm{mA}$.

Figure 4.8. Produced ground electrode.

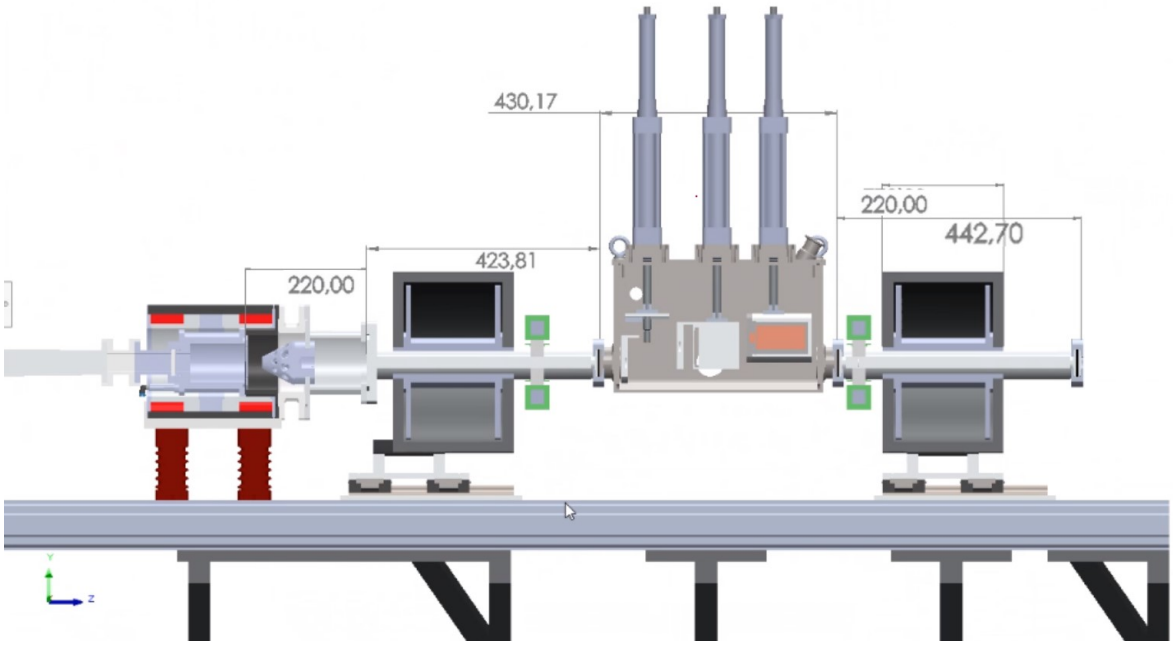

Figure 4.9. The final configuration of the LEBT line which includs the PM-MDIS with its dual-electrode extraction unit and the MBOX between two solenoids, two steerer electromagnets.

4.2.1. Trajectory Analysis for H_2^+ and H_3^+ Ions in LEBT Line

How the dihydrogen and trihydrogen cation ions will affect the beam transmission efficiency needs to be examined. These ions are likely to occur and be extracted from an ion source besides H^+, even at low rates in proton fraction. They might hit the beam pipe, therefore cause electron emission and deterioration of the vacuum environment. Simulations have been conducted separately for each of these low-fraction ions at the same current density with H^+. Simulation results of extraction and transmission are shown in Figures 4.10 and 4.11. The area under the loss curve is considered to calculate the total loss. The transmission losses are rather negligible even at $180\,\mathrm{A/m^2}$ current density. Conducting simulations at such high density gives the worst-case scenario by assuming the entire beam is composed of the selected type of ion.

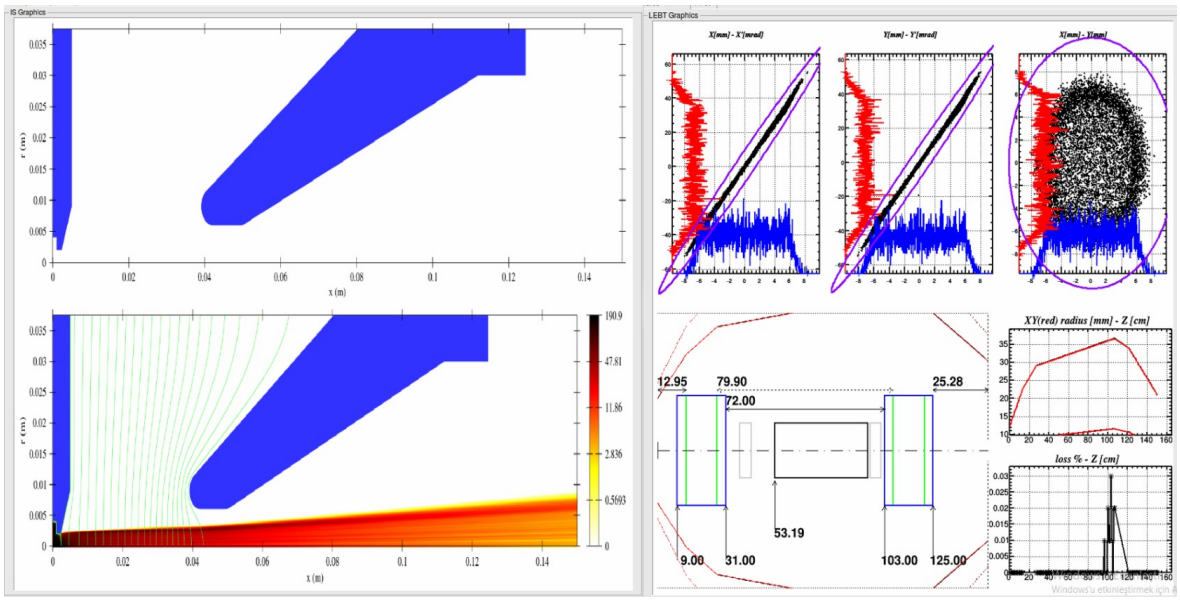

Figure 4.10. Beam trajectory for H_2^+ (dihydrogen cation) ions for current density = $180\,\mathrm{A/m^2}$.

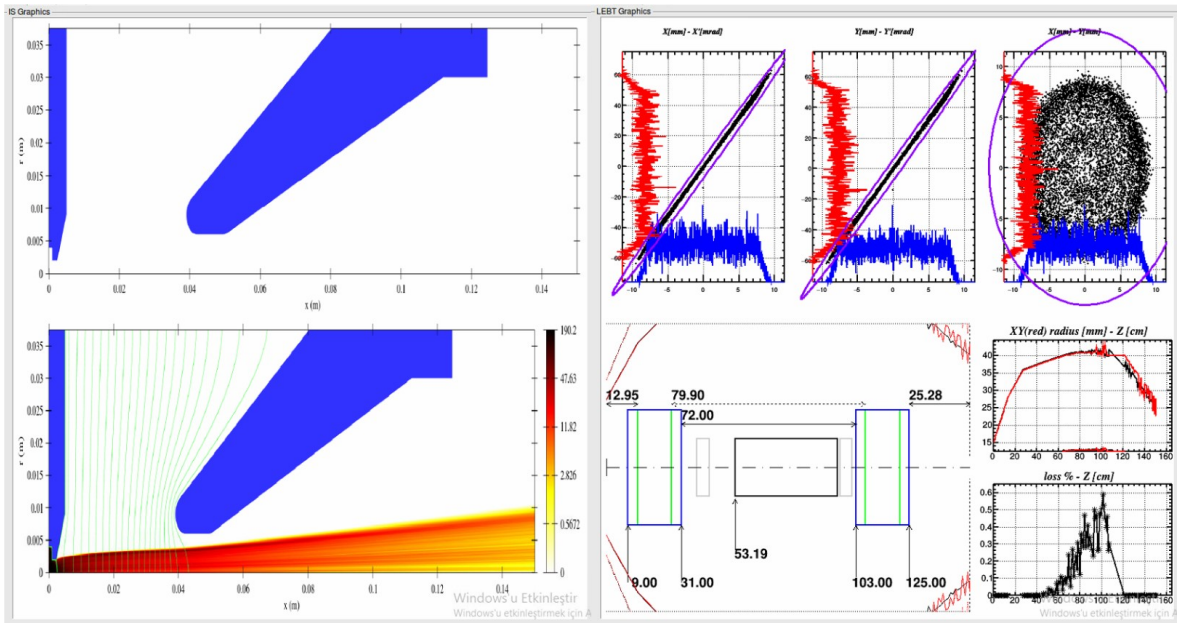

Figure 4.11. Beam trajectory for H_3^+ (trihydrogen cation) ions for current density = $180\,\mathrm{A/m^2}$.

Proton fraction of a microwave discharge ion source has been taken from the literature. More than 90% of the incoming beam is formed from H^+, ∼7% is from H_2^+, and ∼3% is from H_3^+ [32]. This data is used as input current density in IBSIMU simulations.

Results of the simulation studies are summarized in Table 4.1. As it can be seen, the loss values for H_2^+ and H_3^+ are still higher than the loss of H^+ despite its 90% fraction. It is consistent with the observations in the cited study. It has been found as H_2^+ and H_3^+ are less affected by the focusing magnetic field and get dispersed when they are compared with H^+ ions.

Table 4.1. Loss and beam current results at the realistic current densities.

Ion Type	Current Density (A/m^2)	Beam Current (mA)	RMS Loss (%)
H^+	180	1.3	∼0
H_2^+	18	0.19	∼1.8
H_3^+	5	0.06	∼0.2

For the LEBT setup in this study, the effect of the high charge state ions has been found negligible. Despite the insignificant loss, if it is still required to dissociate these ions from the proton beam, an analyzing magnet can be designed and placed to the beamline. Another option to eliminate losses of these ions is to increase the LEBT beampipe diameter from 5cm to 7cm. As it can be seen from Figures 4.12 and 4.13, the loss is reduced to 0% for RMS by increasing the diameter of the beampipe.

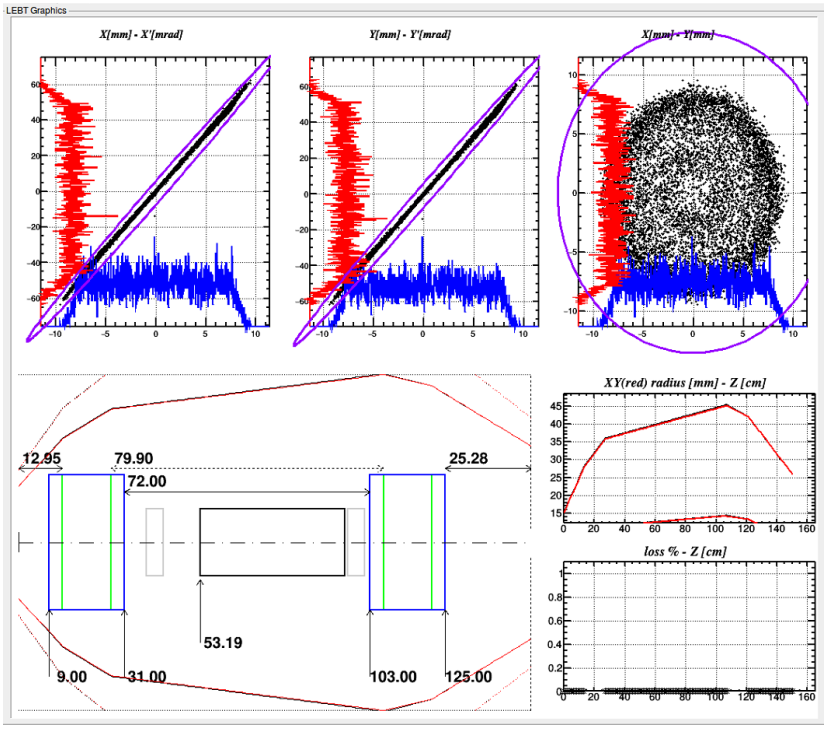

Figure 4.12. Beam trajectories for H_2^+ ions. Beampipe diameter = 7 cm.

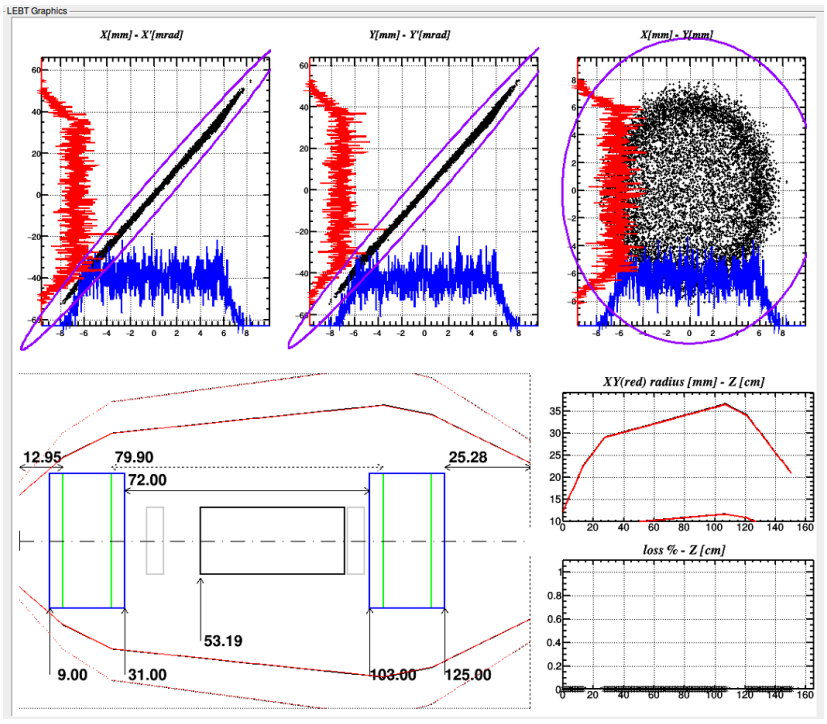

Figure 4.13. Beam trajectories for H_3^+ ions. Beampipe diameter = 7 cm.

5. PM-MDIS INITIAL BEAM RESULTS

After the successful completion of the design, production, magnet assembly, and magnetic field measurements; beam tests are performed with the new PM-MDIS, including the ion extraction system.

5.1. Vacuum Tests

Beam tests are started by performing vacuum tests at the first stage. Before starting the vacuum tests, all the components are cleaned using alcohol to prevent contamination from production. And then, vacuum tests are performed only on the plasma chamber initially before performing on the entire system to detect possible vacuum leaks step by step. In Figure 5.1, vacuum test of the plasma chamber is shown. Vacuum tests are performed using a turbomolecular vacuum pump.

Figure 5.1. Plasma chamber vacuum test using turbomolecular vacuum pump.

After the plasma chamber vacuum tests have been completed, the whole system is assembled, and the tests are repeated. No leakage has been observed and the vacuum value has been found as 6.3×10^{-5} mbar for the first run that is suitable to continue the beam tests. In the later experiments, the lower vacuum values have also been obtained.

5.2. HV Tests

After the vacuum test of the system has been completed, HV tests are conducted to determine if there is a voltage leakage. Detection of any voltage leakage is quite critical in accelerator systems because HV can damage other devices, such as current sources, vacuum pumps, or control systems, as well as cause serious injury. On the other hand, when there is a spark between the two electrodes, the beam with the desired energy cannot be ejected properly.

While gradually increasing the voltage level up to 20 kV, all the corners of the system have been measured using an HV probe, the HV leakage control setup is shown in Figure 5.2. Between the plasma electrode and the ground electrode, a voltage jump through the air has been detected from the metallic screws used to fix the insulating material. It has been produced and placed a plexiglass cage in this area in a suitable shape and size that will prevent the voltage jump through the air.

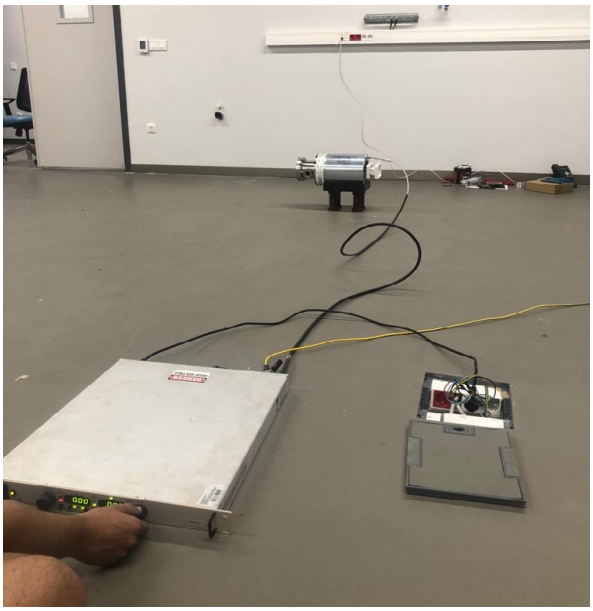

Figure 5.2. HV leakage control setup using Glassman 20 kV high voltage power supply unit.

5.3. Beam Tests

The new PM-MDIS system is finally integrated to the magnetron circuit and microwave transmission waveguide system. It is tested with 0.01 standard cubic centimeter per minute (sccm) hydrogen gas under 20 kV voltage difference and 4×10^{-5} mbar vacuum pressure. A proton beam can be obtained in the first tests with that initial configuration.

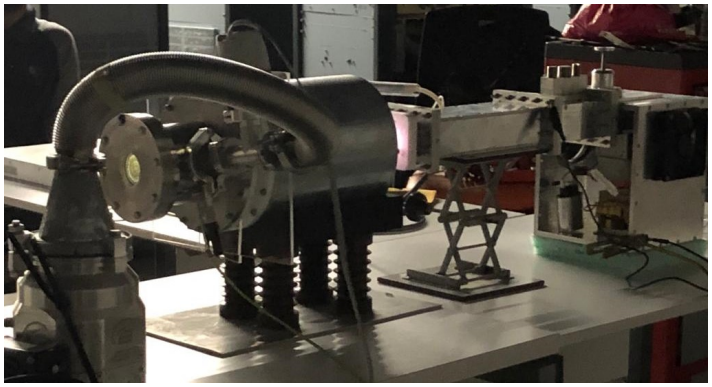

Figure 5.3. Magnetron circuit and microwave transmission waveguide system, hydrogen plasma visible in pink at the end of the waveguide line, and PM-MDIS operating under 20 kV voltage.

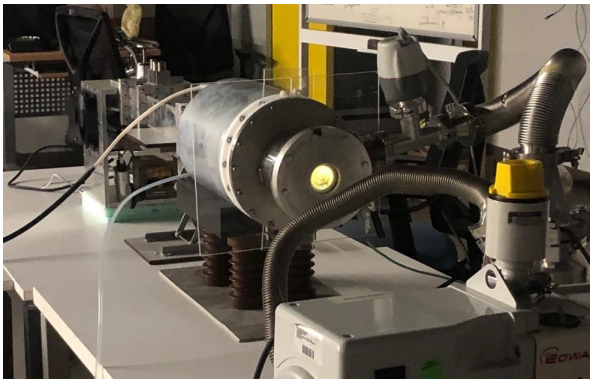

Figure 5.4. Beam visible through fluorescent screen placed at the end of the operating PM-MDIS.

The operating PM-MDIS with magnetron circuit and microwave transmission waveguide system are shown in Figures 5.3 and 5.4.

The results of the experiments mentioned in this section, have all been performed at 20 kV voltage difference. In Figure 5.5, the obtained beam image from the fluorescent screen placed at the end of our new ion source system is shown. The beam image taken from an old oscilloscope screen, which is attached to observe beam instead of the fluorescent screen, is seen in Figure 5.6.

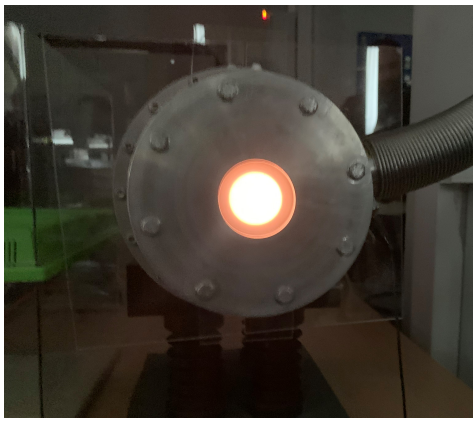

Figure 5.5. The obtained beam image from the fluorescent screen placed at the end of the PM-MDIS system.

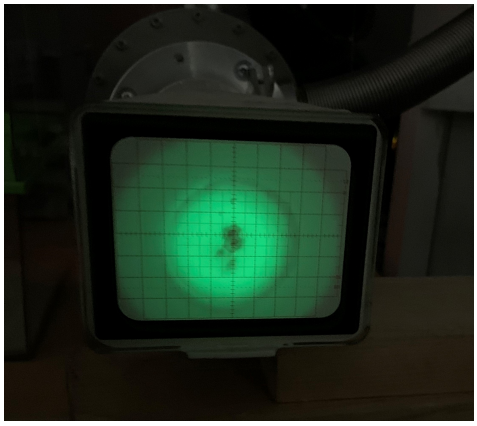

Figure 5.6. The obtained beam image from the oscilloscope screen placed at the end of the PM-MDIS system.

Then, the PM-MDIS has been integrated to the proton beamline, which includes the LEBT line consisting of focusing and defocusing electromagnets around the beampipe, and the MBOX between the electromagnets. The overall system after integrating PM-MDIS to the beamline can be seen in Figure 5.7. During the initial beam test with the PM-MDIS and the LEBT line, the currents of the electromagnets are adjusted to 14.85 A and 6.5 A, respectively. The beam image from the fluorescent screen placed at the end of the LEBT line is given in Figure 5.8. The mean current value read from the HV PSU during these experiments is 0.35 mA.

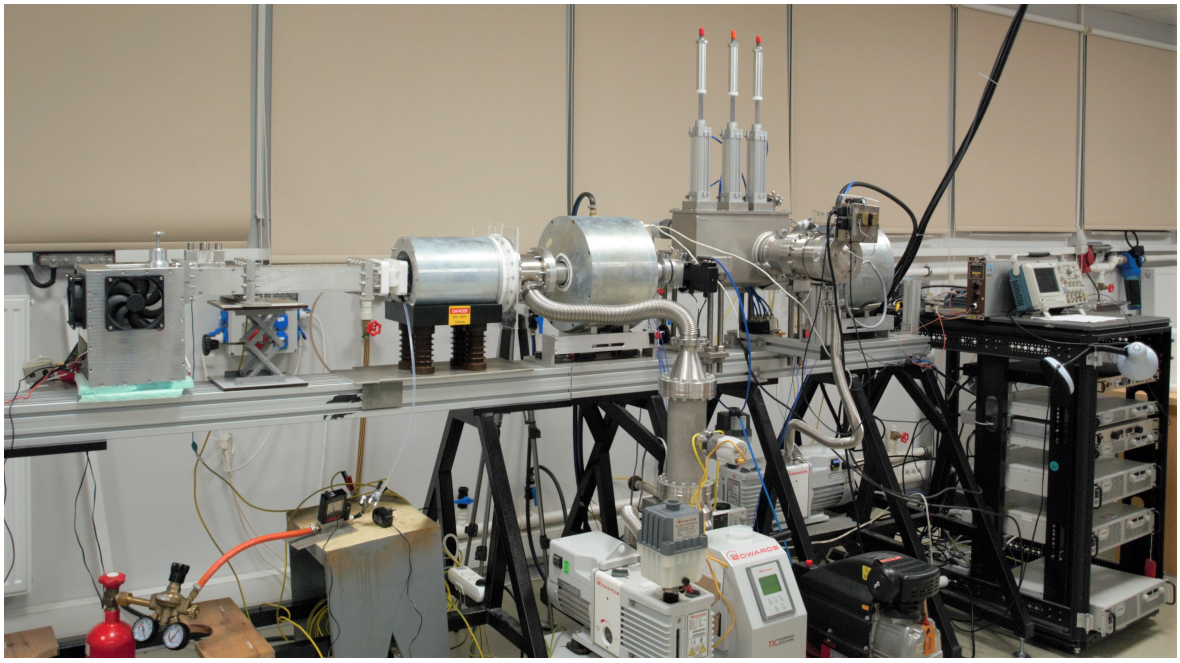

Figure 5.7. Overall setup after integrating the PM-MDIS into the proton beamline, which consists of the ion source setup with microwave transmission unit, and the LEBT line including electromagnets and MBOX.

The beam current results obtained with an oscilloscope, connected to the Faraday cup with the measurement circuit, are given in Figure 5.9. Faraday cup design has a bias electrode that prevents the escape of the secondary electrons. The bias voltage is kept at 0 V while the Faraday cup voltage is kept at the ground. Duty factor, which means the ratio of the pulse width to the its period and is calculated using the formula

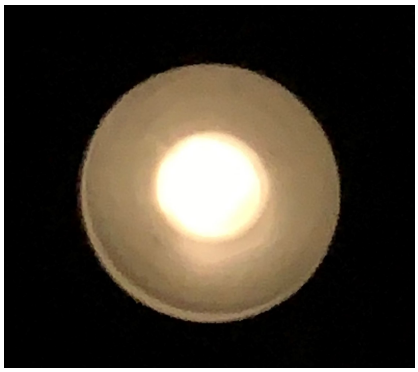

Figure 5.8. The beam image from the fluorescent screen at the end of the LEBT line.

Figure 5.9. The beam current results measured at 20 kV using the Faraday cup connected to an oscilloscope.

$t_{on}/(t_{on} + t_{off})$, is found as 46%. The mean voltage is calculated as

$$V_{peak} \times 46\% = V_{mean} \tag{5.1}$$

where V_{peak} is peak voltage, it is read as 9.40 V read from oscilloscope screen in Figure 5.9, but the peak is not stable along the pulse. Thus we calculated the peak voltage as 8.3 V using weighted average formula. Hence we find, $V_{mean} = 3.8\,V$. We can then obtain the mean current, I_{mean}, as

$$I_{mean} = \frac{V_{mean}}{R} \tag{5.2}$$

where R is resistance, which is 10k Ω for our Faraday cup circuit. In this study carried out to test the operation of the device, the mean current read from the HV PSU is 0.35 mA and the mean current read from the Faraday cup through the oscilloscope is found as 0.38 mA when the bias voltage is 0 V. The relative difference between these two values is about 8%. Considering that this is the initial beam test, that the average beam current read from the Faraday cup is deemed compatible with the current read from the HV PSU.

6. CONCLUSION

In this thesis, a new permanent magnet microwave discharge ion source (PM-MDIS) operated with 2.45 GHz source has been designed, constructed and tested. The PM-MDIS design mainly includes a dual-electrode extraction unit which has been designed in accordance with magnetic field profile of the permanent magnet configuration, a microwave transmission system with 2.45 GHz magnetron. The existing LEBT line at the ion extraction point of the PM-MDIS has also been reconfigured according to the new system specifications.

On the other hand, the trajectory analysis for the H_2^+ and H_3^+ ions has been conducted. The effect of these higher charge state ions, which is not subject to our beamline, has been found negligible. If it is still required to dissociate these ions from the proton beam, an analyzing magnet can be designed and placed to the beamline.

After the construction of the new PM-MDIS system, including its electrode extraction unit, its HV, vacuum, and beam tests have been completed before being integrated into the beamline system. Finally, the PM-MDIS has been successfully operated, and 0.38 mA mean beam current has been measured with the Faraday cup in the experiments performed at 20 kV and 0.01 sccm gas flow.

REFERENCES

1. Karatay, A., A. Çağlar, A. Adiguzel, B. Baran, O. Cakir, S. Öz, Önder Yılmaz, E. Celebi, H. Cetinkaya, S. Esen, U. Kaya, O. Kocer, E. Ozcan, G. Turemen, G. Unel and F. Yaman, "PTAK 800 MHz Proton Radyo Frekans Dört Kutuplusunun (RFQ) Tasarımı ve Test Üretiminde Gelinen Nokta", *Local Infrastructure and R&D Workshop for Particle Accelerators and Detectors, Istinye University Vadi Campus, Istanbul*, 2021.

2. Bailey, R. (Editor), *Proceedings, CAS - CERN Accelerator School: Ion Sources: Senec, Slovakia*, CERN Accelerator School, CERN, Geneva, 2013.

3. Miracoli, R., *Characterization Of Microwave Discharge Ion source For High Proton Beam Production In Cwand Pulsed Mode*, Ph.D. Thesis, University of Catania, 2010.

4. Celona, L., "Microwave Discharge Ion Sources", pp. 421–441. 21 p, 2014, arXiv:1411.0538, Contribution to the CAS-CERN Accelerator School: Ion Sources, Senec, Slovakia, edited by R. Bailey.

5. Yong-Sub, C., K. Dae-Il, K. Hyeok-Jung, S. Kyung-Tae and K. Han-Sung, "Microwave Ion Source with a Permanent Magnet Solenoid", *Journal of Korean Physical Society*, Vol. 59, pp. 586–589, 2011.

6. Cetinkaya, H., E. Algin, G. Turemen, U. Dogan and L. Sahin, "A Cost Effective Microwave Ion Source Test Stand", *IEEE Transactions on Plasma Science*, Vol. 48, No. 6, pp. 2132–2137, 2020.

7. Scrivens, R., "Classification of Ion Sources", p. 18 p, 2014, contribution to the CAS-CERN Accelerator School: Ion Sources, Senec, Slovakia, Edited by R. Bailey, CERN-2013-007.

8. Brown, I., "The Physics and Technology of Ion Sources, Second Edition", *The Physics and Technology of Ion Sources, Second, Revised and Extended Edition, by Ian G. Brown (Editor), pp. 396. ISBN 3-527-40410-4. Wiley-VCH.*, Vol. -1, 2004.

9. Leung, K., *Radio Frequency Driven Ion Sources*, pp. 163 – 175, 2005.

10. Chen, W., H. Li, R. L. Zhu, K. J. Xue, X. Cao, Y. J. Lü, S. J. Liu, Y. C. Xiao, S. M. Liu and H. F. Ouyang, "Operation of RF Driven Negative Hydrogen Ion Source In China Spallation Neutron Source", *Review of Scientific Instruments*, Vol. 90, No. 11, p. 113320, 2019.

11. Gammino, S., *Production of High Intensity, Highly Charged Ions*, CERN, 2014.

12. Geller, R., "ECRIS: The Electron Cyclotron Resonance Ion Sources", *Annual Review of Nuclear and Particle Science*, Vol. 40, No. 1, pp. 15–44, 1990.

13. Çetinkaya, H., *Prototype Ion Source Design Intended for Turkish Accelerator Center Proton Accelerator Facility*, Ph.D. Thesis, Dumlupınar University, 2016.

14. Sakudo, N., K. Tokiguchi, H. Koike and I. Kanomata, "Microwave Ion Source for High Current Implanter", *Review of Scientific Instruments*, Vol. 49, No. 7, pp. 940–943, 1978.

15. Taylor, T. and J. S. Wills, "A high Current Low Emittance DC ECR Proton Source", *Nuclear Instruments and Methods in Physics Research Section A: Accelerators, Spectrometers, Detectors and Associated Equipment*, Vol. 309, No. 1, pp. 37–42, 1991.

16. Sakudo, N., "Microwave Ion Sources for Industrial Applications", *Review of Scientific Instruments*, Vol. 71, p. 1016–1022, 2000.

17. Popov, O. A., "Effects of Magnetic Field and Microwave Power on Electron Cyclotron Resonance Type Plasma Characteristics", *Journal of Vacuum Science & Technology A*, Vol. 9, No. 3, pp. 711–716, 1991.

18. Systèmes, D., "Hollow Rectangular Waveguide Simulation", 3ds.com/products-services/simulia/resources/hollow-rectangular-waveguide/.

19. *Reference Manual for the Poisson/Superfish Group of Codes*, 1987, https://www.osti.gov/biblio/10140827.

20. *Data Sheet Article Q-60-30-15-N*, www.supermagnete.de, november 2011.

21. Hunter, J. D., "Matplotlib: A 2D Graphics Environment", *Computing in Science & Engineering*, Vol. 9, No. 3, pp. 90–95, 2007.

22. Gerling Applied Engineering, Inc., *Pressure/Vacuum Window, WR284*, 7 2009.

23. Kalvas, T., "Beam Extraction and Transport", pp. 537–564. 39 p, 2014, arXiv:1401.3951, CERN Accelerator School CAS.

24. Kilpatrick, W. D., "Criterion for Vacuum Sparking Designed to Include Both RF and DC", *Review of Scientific Instruments*, Vol. 28, pp. 824–826, 1957.

25. Coupland, J. R., T. S. Green, D. P. Hammond and A. C. Riviere, "A Study of the Ion Beam Intensity and Divergence Obtained from a Single Aperture Three Electrode Extraction System", *Review of Scientific Instruments*, Vol. 44, No. 9, pp. 1258–1270, 1973.

26. Edwards, D. A., M. J. Syphers and W. Barletta, "Introduction to the Physics of High Energy Accelerators", *Physics Today*, Vol. 47, No. 2, pp. 99–99, 1994.

27. Kalvas, T., O. Tarvainen, T. Ropponen, O. Steczkiewicz, J. Ärje and H. Clark, "IBSIMU: A Three Dimensional Simulation Software For Charged Particle Optics", *Review of Scientific Instruments*, Vol. 81, No. 2, p. 02B703, 2010.

28. Cakir, O., E. Celebi, H. Cetinkaya, H. Kolenoglu, G. Turemen, Z. Uysal and G. Unel, "DemirciPro's Tools for Completing the Linac: Ion Source and LEBT Line", e-print arXiv:2103.11829v2, 2021.

29. Brun, R., F. Rademakers, P. Canal, A. Naumann, O. Couet, L. Moneta, V. Vassilev, S. Linev, D. Piparo, G. GANIS, B. Bellenot, E. Guiraud, G. Amadio, wverkerke, P. Mato, TimurP, M. Tadel, wlav, E. Tejedor, J. Blomer, A. Gheata, S. Hageboeck, S. Roiser, marsupial, S. Wunsch, O. Shadura, A. Bose, CristinaCristescu, X. Valls and R. Isemann, "Root-Project/Root: v6.18/02", Zenodo, 2019.

30. Perrin, A., T. Mütze, J. Amand and J. Lallement, *Travel v4.07 User Manual*, 2007.

31. Açıksöz, S., A. Adıgüzel, H. Çetinkaya, S. Esen, D. Halis, A. Hamparsunoğlu, T. B. İlhan, A. Kılıçgedik, O. Koçer, S. Oğur, S. Öz, A. Özbey, V. E. Özcan and N. G. Ünel, "Beam Diagnostics at KAHVELab Proton Source and LEBT Line", *PoS*, Vol. EPS-HEP, p. 856, 2022.

32. P.Roychowdhury, H.Kewlani, L.Mishra, S.Gharat and R.K.Rajawat, "Emittance and Proton Fraction Measurement in High Current Electron Cyclotron Resonance Proton Ion Source", *Nuclear Instruments and Methods in Physics Research*, Vol. 795, pp. 45–51, 2015.

33. Chen, F. F., *Introduction to Plasma Physics and Controlled Fusion*, Springer Cham, 2016.

34. Çınar, K., *Design and Construction of a Microwave Plasma Ion Source*, M.S. Thesis, Middle East Technical University, 2011.